Chapter 10

Electrodeposited Zinc-Nickel Nanocomposite Coatings

Heidi Conrad and Teresa D. Golden

Additional information is available at the end of the chapter

http://dx.doi.org/10.5772/intechopen.80219

Abstract

Composite coatings can demonstrate improved property performance as compared to metals and alloy materials. One category of composite coatings is composed of metal or metal alloys with a dispersed phase of nonmetallic nanoparticles. The addition of these nanoparticles has been found to improve corrosion, wear resistance, and hardness. Producing metal composite coatings using electrochemical techniques can be advantageous due to reduced production cost, lower working temperatures, and precise control of experimental parameters. Metal coatings such as zinc have been successfully co-deposited with TiO_2, SiO_2, CeO_2 and mica particles and nickel has been co-deposited with a number of materials including TiO_2, SiC, Al_2O_3, PTFE and silicates. Zinc-nickel alloys have long been studied for a number of properties, most notably corrosion resistance and recently their tribological properties. This chapter reviews the literature on electrodeposition of ZnNi nanocomposite coatings. Although there has been much work done on composite coatings, there is much less literature available on composite coatings with zinc-nickel alloys. So in this review, we look at the general trends for nanoparticle incorporation, deposition mechanisms, system stability, microstructures of the coatings and general corrosion trends.

Keywords: electrodeposition, alloys, nanocomposites, corrosion, Zn-Ni alloys, metal matrix composites

1. Introduction

Metal matrix composite (MMC) coatings are promising materials developed by inclusion of a dispersed reinforcing material into a metal matrix. MMC's can replace traditional materials through their ability to offer improved mechanical and physical properties such as increased hardness, wear resistance, low thermal expansion coefficients, lubrication properties, antibacterial properties and improved corrosion resistance [1–11]. Nanosized particle incorporation

IntechOpen

© 2018 The Author(s). Licensee IntechOpen. This chapter is distributed under the terms of the Creative Commons Attribution License (http://creativecommons.org/licenses/by/3.0), which permits unrestricted use, distribution, and reproduction in any medium, provided the original work is properly cited. CC BY

in metal matrixes forms a nanocrystalline structure, leading to improved properties of the material due to modification of the growth of the deposit [7, 12]. The properties of the composite coating are dependent on concentration, size, distribution and type of nanoparticle incorporated, in addition to the method and parameters used during coating formation [13, 14]. Although there are a large number of successful metal/particle combinations, this review will focus on zinc-nickel nanoparticle coatings exclusively. Individually nickel has been successfully co-deposited with a number of materials including TiO_2, SiC, Al_2O_3, PTFE and layered silicates such as montmorillonite (Mt) [2, 7, 15–19] and zinc has been successfully co-deposited with TiO_2, CeO_2, ZrO_2, SiO_2, mica particles and polymeric nano-aggregates (PNAs) [20–25] but a review of current literature on ZnNi alloy nanocomposite coatings has not been compiled to our knowledge. An overview of the literature is shown in **Table 1**. The most commonly used reinforcement material for zinc-nickel coatings is Al_2O_3 constituting ~32% of the papers, followed by TiO_2 and SiO_2/SiC with ~20% each, carbon nanotubes and CeO_2 with ~8% each, and Al_2O_3/SiC, CeO_2/SiO_2 and Mt with ~4% each [11–13, 26–48].

Zinc-nickel coatings are well known in the field of corrosion resistance as a corrosion resistant material. Corrosion protective coatings are commonly used to extend the lifetime of materials such as stainless steel from corrosion onset as a substitute for more expensive, less available materials [49–53]. Coating zinc onto stainless steel, known as galvanization, is an industry standard to protect against corrosion. The zinc coating sacrificially corrodes, thereby protecting the stainless steel from corrosion [54–56]. Options are now being explored to withstand harsher conditions, longer lifetimes, reduced thickness and better overall strength of the protective coating layer. Although a large focus has been on the development of generalized corrosion resistant coatings, when considering cost, environmental impact and performance,

Reference and application	Plating bath	Incorporated particle and deposition parameters	Dispersion method
Blejan et al. [17] Corrosion	106 g/L ZINCATE 75 (75 g/L Zn and 400 g/L NaOH), 12 mL PERFORMA 285 Ni-CPL, 100 mL PERFORMA Additive K. 82.6 g/L NaOH, pH = 13	Al_2O_3 60 nm powder, S.A. 74 m^2/g 5, 10, 15 g/L 2 A/dm^2, 23 ± 2°C	Ultrasonication and solution stirring during deposition.
Ghaziof et al. [33, 34] Corrosion, microhardness	35 g/L $ZnSO_4 7H_2O$, 35 g/L $NiSO_4 6H_2O$, 80 g/L Na_2SO_4, pH = 4	Alumina Sol 6 mL/L $i_{DC} = i_{avg.} = 80$ mA/cm^2 $i_{peak} = 160$ mA/cm^2 Frequency (HZ) = 100 ($t_{on} = T_{off} = 5$ ms), 500 ($t_{on} = t_{off} = 1$ ms) 40°C	Bath agitated 10 min prior to deposition.
Ataie et al. [35] Tribological properties	150 g/L $ZnCl_2$, 250 g/L $NiCl_2 6H_2O$, 45 g/L H_3BO_3, 100 g/L KCl, 100 g/L NH_4Cl, 0.1 g/L SDS, pH = 4	α-Al_2O_3 ~30 nm 15 g/L 18 a/dm^2, 30°C	Magnetic stirring 24 h prior to deposition, 500 rpm. Sonicated 2 h (500 W) (15 min on, 15 min off for 2 h). Magnetic stirring during deposition, 250 rpm simultaneously with sonication.

Reference and application	Plating bath	Incorporated particle and deposition parameters	Dispersion method
Shourgeshty et al. [36, 37] Corrosion, wear properties	250 g/L $ZnCl_2$, 150 g/L $NiCl_2 6H_2O$, 45 g/L H_3BO_3, 100 g/L KCl, 100 g/L NH_4Cl, 0.5 g/L, pH = 4 ± 0.5	α-Al_2O_3 ~20 ± 5 nm 15 g/L 4 A/dm^2, 30 ± 2°C	Magnetic stirring 12 h prior to deposition, 300 rpm, followed by 1 h ultrasonication (250 W, 20 KHz). During deposition mechanical stirring, 150 rpm and ultrasonic waves (50 W, 20 KHz).
Zheng et al. [38, 39]	60 g/L $ZnCl_2$, 120 g/L $NiCl_2 6H_2O$, 120 g/L KCl, 100 g/L NH_4Cl, 30 g/L $NaCH_3COO$, pH = 5.0	α-Al_2O_3, particle diameter ~100 nm 50 g/L 4 A/dm^2, 35 ± 1°C	Magnetic stirring 24 h, 2000 rpm prior to deposition. Ultrasound generator and mechanical stirring (200 rpm) during deposition.
Momeni et al. [14] Hardness, antibacterial properties	57.5 g/L $ZnSO_4 7H_2O$, 52.5 g/L $NiSO_4 6H_2O$, 9.3 g/L H_3BO_3, 56.8 Na_2SO_4, 0.53 H_2SO_4, pH = 2.5	TiO_2 0.0–3.0 g/L 1 A/dm^2, 35°C	Stirring during deposition, 500 rpm.
Gomes et al. [40, 41]	0.10 M $ZnSO_4 7H_2O$, 0.30 M $NiSO_4 6H_2O$, 0.20 M $MgSO_4$, 0.15 M H_3BO_3, pH = 4	TiO_2, particle size ~25 nm 10 g/L –3.2 A/dm^2, Room Temp	Ultrasonic agitation 30 min prior to deposition. Stirring during deposition, 400 rpm.
Katamipour et al. [42] Corrosion, mechanical	60 $ZnCl_2$, 120 g/L $NiCl_2 6H_2O$, 120 KCl, 100 NH_4Cl, 30 $NaCH_3COO$, pH = 4.6	TiO_2, ~25 nm 3 g/L 3.5 A/dm^2, 35 ± 1°C	Magnetic stirring, 1500 rpm 24 h prior to deposition. Ultrasound generator and stirring during deposition, 600 rpm.
Praveen et al. [43] Corrosion	160 g/L $ZnSo_4 7H_2O$, 16 g/L $NiSO_4 6H_2O$, 12 g/L H_3BO_3, 40 g/L Na_2SO_4, 1.5 g/L cetyl trimethyl ammounium bromide, pH = 4	TiO_2, ~100–200 nm 3 g/L 2 A/dm^2, 27°C	Magnetic stirring 10 h prior to deposition.
Tuaweri et al. [30, 44] Corrosion	57.5 g/L $ZnSO_4 7H_2O$, 131 g/L $NiSO_4 6H_2O$, 162 $Na_2SO_4 10H_2O$, pH = 2.0–2.5	SiO_2 13–52 g/L 1–10 A/dm^2	Agitation through use of vibro-agitation with vibromixer prior to deposition.
Ullal et al. [45] Corrosion	100 g/L $ZnSO_4 7H_2O$, 100 g/L $NiSO_4 6H_2O$, 75 g/L $NaCH_3COO 3H_2O$, 2 g/L citric acid, 0.5 g/L thiamine hydrochloride, pH = 3.0 ± 0.05	SiO_2 nanopowder 5 g/L Deposition current and temp—not specified	Magnetic stirring 24 h prior to deposition. Agitation of solution with circulation pump during deposition.
Takahashi et al. [46]	1 M $ZnSO_4 7H_2O$, 0–0.7 M $NiSO_4 6H_2O$, pH = 2.0	SiO_2 colloid (Cataloid SN) 0–300 g/L 100 A/dm^2, 50°C	Not specified
Poliak et al. [47] Mechanical properties	125 g/L $ZnSO_4 7H_2O$, 75 g/L $NiSO_4 6H_2O$, 25 g/L H_3BO_3, pH = 4	SiO_2 powder, ~10 nm 1 g/L 2A/dm^2	Not specified

Reference and application	Plating bath	Incorporated particle and deposition parameters	Dispersion method
Müller et al. [48]	0.16 M ZnO, 1.7×10^{-2} $NiSO_4 6H_2O$, 3.75 M NaOH, 3.4×10^{-2} M diethylenetriamine, pH = alkaline	α-SiC powder, ~7.0 μm 20–120 g/L 25°C	Stirring 24 h prior to deposition, substrate rotated during deposition.
Creus et al. [49, 50] Corrosion	63 g/L $ZnCl_2$, 100 g/L $NiSO_4 6H_2O$, 215 g/L KCl, 20 g/L H_3BO_3, pH = 5.3.	CeO_2, ~80 nm 5 g/L Cathodic pulse, $i_p = 5.0$ A/dm^2 with $t_{on} = 4$ ms, $t_{off} = 16$ ms. Anodic pulse, $J_a = 1.0$ A/dm^2 with $t_{on} = 4$. Average current density ~0.67 A/dm^2. ms, 25°C	Stirred 24 h prior to deposition, continued stirring during deposition, 200 rpm.
Tseluikin et al. [18, 51]	10 g/L ZnO, 50 g/L $NiCl_2 6H_2O$, 220 g/L NH_4Cl, 20 g/L $NaCH_3COO$	Carbon nanotubes 0.05 g/L Reversing mode, $i_c = 6$ A/dm^2, $i_a = 1.5$ A/dm^2.	Not specified
Tulio et al. [52]	0.25 M $ZnSO_4 7H_2O$, 0.2 M $NiSO_4 6H_2O$, 0.4 M H_3BO_3, 0.1 M sodium citrate, pH = 4.9.	α-SiC ~9.5 μm, α-Al_2O_3 ~3.4 μm Not specified 25°C	Stirred 12 h prior to deposition. Substrate rotated during deposition.
Xiang et al. [53] Corrosion	Not specified	CeO_2 modified SiO_2, 400–500 nm Not specified Deposition current and temp—not specified	Not specified
Conrad et al. [54] Corrosion	0.2 M $ZnSO_4 H_2O$, 0.1 M Ni$(NH_4)_2(SO_4)_2 6H_2O$ 0.1 M $Na_2B_4O_7 10H_2O$ pH = 9.5	Montmorillonite (Mt) 1, 5 g/L $E_1 = -1.45$ V, $T_1 = 10$ sec. $E_2 = -0.9$ V, $T_2 = 2$ sec, Room Temperature	Sonicated 1 h prior to deposition, N_2 gas bubbled through solution during deposition.

Table 1. Survey of literature.

zinc alloys have become an attractive option. An alloy modifies the composition of a material resulting in different corrosion properties then the original element which can significantly improve the stability of the protective coating [2–5, 52, 57, 58], therefore, by picking the correct combination of alloys, one can greatly increase the corrosion resistance of the material [49, 52]. Alloy formation can result in various phases, dependent upon the experimental conditions at the time of formation. For zinc-nickel, there are 5 known alloy phases: α- and β- (30% Ni, nickel rich), γ- (Ni_5Zn_{21}), δ- (Ni_3Zn_{22}) and η- (1% Ni) (zinc rich), all dependent upon the Zn/Ni ratio and experimental parameters used to form the alloy [50, 55, 59–61]. The γ-phase and δ-phase are predominantly formed through electrochemical methods, with γ-phase showing the strongest protection against corrosion [57, 60, 62–65]. Zinc nickel γ-phase alloys with approximately 8–18% have been found to be optimal for maximum corrosion protection [48, 57, 62, 65].

Although several methods are available for the development of nanocomposite coatings, electrodeposition remains a favorable choice due to relative ease of use, low cost, convenience, ability to work at low temperatures and overall control of experimental parameters [39, 48, 58, 65]. A general survey of the literature concerning zinc-nickel nanocomposite coatings found electrochemical deposition to be the main preparation method, so general trends and properties of the coatings formed through electrochemical methods will be the focus of this chapter.

2. Electrodeposition of zinc-nickel nanocomposite coatings

2.1. Dispersion of particles

A variety of particles, including Al_2O_3, TiO_2, SiO_2, SiC, ceria, carbon nanotubes and montmorillonite (Mt) have been successfully incorporated into zinc-nickel coatings. For optimal effect, the nanoparticles need to be dispersed throughout the metallic coating. To accomplish this, the particles first need to be suspended in the electrolytic solution and agglomeration of the particles needs to be kept to a minimum to prevent issues in coating formation. Particle agglomeration is an issue seemingly independent of particle concentration as it occurs under low to high concentrations, though smaller particle size does increase tendency to form agglomerations, leading to less incorporation in the final coating. To prevent agglomeration, various methods can be used such as organic additives, agitation of the solution, current density, etc. Treatment of the nanoparticles prior to deposition is varied throughout the field but the most common methods used for particle suspension are magnetic stirring, sonication or a combination of stirring and sonication prior to and during deposition [11–13, 26–48]. In addition to treatment of the nanoparticles, concentration in the bath also affects the quality of the coatings. As expected, as the concentration of nanoparticles in the bath increases, the concentration of nanoparticles in the resulting coating tends to increase. The small sized particles are easily incorporated into irregularities on the metal surface and positively charged particles are attracted to the cathode, so more easily incorporated into the coating [13]. In the case of oxide nanoparticles, the oxides compete with the metallic ions for adsorption onto the active sites, creating more nucleation sites and perturbing metallic grain growth. Other particles are trapped during deposition, filing holes or gaps within the naturally forming coating [22, 40].

Concentration of nanoparticles in the bath varies from 0.05–300 g/L with most work using around 5–15 g/L. Müller et al., who relied on mechanical stirring to disperse the nanoparticles, found optimal concentration of SiC particles to be 60 g/L, beyond which the particles began to agglomerate. Beyond this concentration, stirring was not sufficient to keep the particles suspended in solution and a decreasing trend of SiC in the coatings was observed [42].

Katamipour et al. studied the effects of ultrasonic conditions to promote uniform dispersion of the coating particles, and to determine if improvement occurred in the corrosion and mechanical properties of the coatings. They found that increasing the ultrasonic power density lead to a decrease in particle size, an increase in nanoparticle incorporation in the coating, and initially, an improvement in corrosion and mechanical properties. The agglomeration often observed with nanoparticles also dissipated with the use of sonication [36]. Nano-alumina

particles were found to be uniformly imbedded in the ZnNi-Al_2O_3 coating after treatment of ultrasonic vibration [32, 33]. Without sonication, ceria nanoparticles were seen organized in long string-shape agglomerates. These agglomerates became trapped inside voids and pores during coating growth [44]. Though sonication or mechanical disruption of the nanoparticles is needed to distribute them throughout the metal matrix, care must be taken as excessive agitation can lead to a lower quality of particles in the deposit [7].

Na-smectites, a type of clay mineral, specifically montmorillonite (Mt) were also examined, for incorporation into metal matrixes. Within aqueous solutions, Na-montmorillonite can be completely exfoliated and incorporated into other materials, forming continuous, crack free films, which is beneficial in corrosion resistant coatings [5, 8–9, 52, 66]. Exfoliation causes the short range order of the clay particles to be disrupted, causing individual clay platelets to exist, unassociated from one another. The resulting clay platelets range 1–2 nm in width with 100–1000 nm in length [66]. These platelets are easily incorporated into the coating during deposition, increasing the overall thermal stability and mechanical strength of the coating, which leads to increased corrosion resistance [2, 8]. As the alloy coating is forming, the exfoliated clay in solution is freely dispersed throughout the electrolytic bath. Mt is a cationic clay with a negatively charged surface which attracts metal ions, increasing incorporation of the platelets into the metal composite during deposition. The clay platelets settle onto the substrate surface as the coating is being formed, allowing them to be incorporated into the coating. Exfoliated Mt, which has a plate-like structure, increases the surface area of the material when imbedded in the coating and leads to a more tortuous mean free path of the corrosion cells upon onset [5]. This technique has previously been successful with the incorporation of montmorillonite platelets into pure nickel, nickel-molybdenum and nickel-copper coatings [2, 5, 8, 9, 52, 58, 66]. However, many traditional particles used in composite coatings are spherical in shape. For example SiO_2 nanoparticles coated with a layer of cerium oxide have been introduced into ZnNi coatings to improve corrosion resistant properties [47].

2.2. Influence of nanoparticle addition on deposition mechanism

Though many researchers use electrochemical deposition as a tool to form a coating of interest, there is little published work on the electrochemical system used for the deposition of zinc-nickel nanocomposite coatings. A better understanding can lead to an improved deposition system, and an overall superior coating. Work continues to be done in acidic and alkaline conditions with a goal of further improving the materials, longer material lifetimes and a better understanding of the mechanisms involved in various alloy formations [49, 50, 55, 57, 59, 60, 65, 67–71] but little work has been done to examine systems with nanoparticle incorporation.

Zinc-nickel alloy formation follows an anomalous deposition mechanism which occurs when the electrochemically less noble metal deposits preferentially to the more noble metal. This is verified through examination of the voltammetry patterns of the zinc-nickel system as the individual zinc and nickel reduction peaks are shifted based on the presence of the other metal species in solution [48, 59, 62, 70, 72–74]. During deposition, a thin layer of nickel is initially deposited onto the substrate. As the deposition continues, zinc is intercalated into the nickel, leading to formation of the alloy [57, 61, 67]. In acidic systems under low current density, a transition from anomalous to normal codeposition has been noted. Normal codeposition is dominant when the

applied potential is more similar to the free corrosion potential of zinc and zinc-nickel alloys. These systems also present with lower current efficiencies [57, 61, 73–77]. Normal deposition leads to alternate ZnNi phases, which are not preferred for maximized corrosion protection, so the goal is to remain under an anomalous deposition route, to further aid in the deposition of γ-phase ZnNi alloy. Within the research presented on the deposition mechanism with nanoparticle presence, the effect of SiO_2, SiC, Al_2O_3, Mt and carbon nanotubes on the deposition mechanism has been explored and is discussed under their individual sections.

Hydrogen evolution at cathodic potentials is a concern in electrochemical deposition as it can lead to the formation of cracks and defects in the overall coating structure, both during deposition and later during use of the material. Hydrogen evolution competes with metal electrodeposition in this system and can play a major role in determining the composition of ZnNi coatings [35, 46]. In ZnNi deposition systems under alkaline conditions, boric acid was found to suppress hydrogen evolution. Hydrogen evolution is a larger concern for nickel deposition than zinc deposition as a larger overpotential is required for nickel deposition since the deposition is under kinetic control while zinc deposition is thermodynamically controlled [57]. Our previous study examined the change in hydrogen evolution onset with varying borate concentrations in alkaline solutions, and found as the borate concentration is increased, hydrogen evolution is pushed to more cathodic values [48]. A maximum borate concentration of 100 mM was used due to conductivity of borate in the system [57]. In addition to borate, nanoparticles can have an overall effect on hydrogen evolution in the system as well. The hydrogen evolution onset was compared for solutions with and without the presence of Mt in **Figure 1**. For nickel, a large cathodic shift was observed when Mt was added to the system. For zinc and zinc-nickel, small cathodic shifts were observed with Mt. The Mt can help further shift the onset of hydrogen evolution within this system, in addition to borate [48, 57]. Alloy formation typically occurs at or near the onset of hydrogen evolution for this system. By shifting the onset in a cathodic direction, less hydrogen will be produced during alloy formation, leading to less entrapped hydrogen in the overall coating. Hydrogen evolution can hinder adsorption of nanoparticles on the surface of the coating material and lead to embrittlement [7].

The addition of Al_2O_3 and SiC was also found to cause a surface blockage preventing hydrogen evolution to occur. This effect is found to be dependent on the concentration of SiC in solution, but for addition of Al_2O_3 no dependency is observed. It is believed that SiC and Al_2O_3 are adsorbed onto the electrode surface, reducing the active surface area. At lower pH, H^+ has a higher tendency to adsorb onto the SiC particles, leading to a reduction in hydrogen evolution [46].

2.3. Deposition methods

Electrodeposition techniques include potentiostatic and galvanostatic deposition, and further into both methods, applied vs. pulsed deposition parameters in the literature for zinc-nickel nanocomposite coatings [44]. The particles co-deposit with the zinc-nickel coating which has advantages over other methods such as better control of coating thickness, deposition speed, working under controlled temperatures, and it is a single-step method. The nanoparticles are incorporated as the metal species are reduced onto the electrode surface, forming the nanoparticle coating. Applied methods include direct current or direct potential, where a constant current or potential is applied to the electrode. Pulsed methods include pulse current

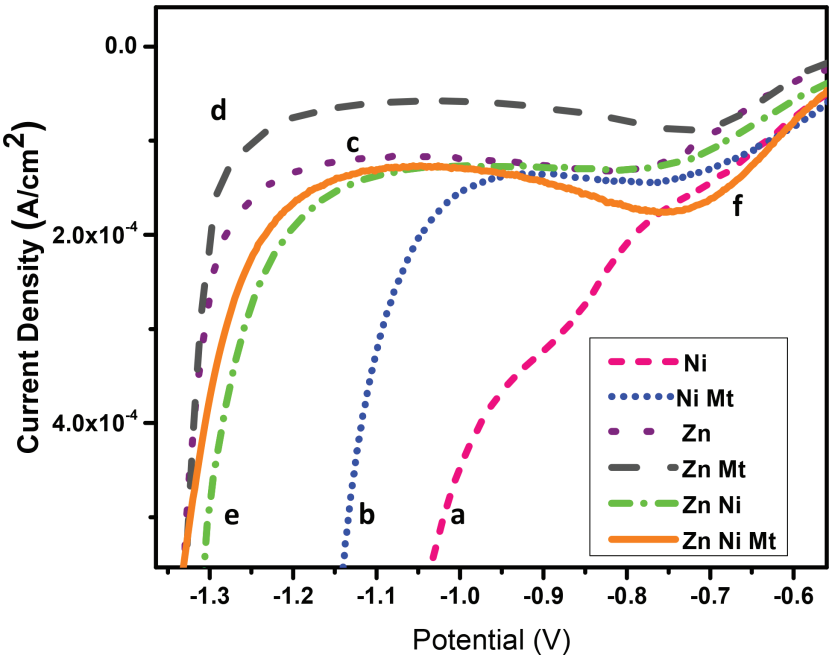


Figure 1. The onset of hydrogen evolution in solutions containing metal salts (specified), Mt (specified) 0.1 M borate and pH = 9.4 with NH_4OH (a) Ni^{2+} (pink short dash); (b) Ni^{2+} Mt (blue dot); (c) Zn^{2+} (purple square dot); (d) Zn^{2+} Mt (black long dash); (e) Zn^{2+}, Ni^{2+} (green dash dot); (f) Zn^{2+}, Ni^{2+} Mt (orange solid) [54].

(PC), pulse reversed current (PRC), pulse potential (PP) and pulse reversed potential (PRP). PC and PP involve alternatively applying two or more cathodic direct current or potentials during the deposition, with off times, when no current or potential is being applied. PRC and PRP are similar to PC and PP as a cathodic pulse is applied but during the off times, an anodic pulse is applied to the electrode. Previous studies show an increase in incorporation of particles through a pulse deposition method with better overall coverage of the underlying material compared to a constant applied potential technique [7, 45, 48, 57, 62, 68, 78–80]. The nanoparticles are incorporated in a higher percentage because of the partial dissolution of the metal deposit during the anodic pulse. Pulse plating was found to improve overall quality of deposits and reduce grain size which inherently increases the corrosion protection of the coating [48, 57–58, 79, 81]. Pulse deposition includes the following attributes: (1) better inclusion of nanoparticles in the metal matrix, (2) lower concentration of nanoparticles needed in the electrolytic solution, (3) selective entrapment based on size of nanoparticles, (4) release of trapped hydrogen prior to coating use which leads to longer coating lifetime and (5) a more opened grain structure which allows hydrogen to escape from the deposit without forming holes or pits in the coatings which could otherwise be used as corrosion cell development sites [7, 48, 57, 80]. Pulsed deposits help embed higher concentrations of nanoparticles because it helps eliminate a fraction of the electrodeposited metal during the off time [7]. Pulse durations affect the shape and size of crystallite formation [21, 81, 82]. During off time,

adsorbed metallic adatoms are able to reorganize and minimize surface energy. The grain growth continues during this time due to desorption of impurities leading to changes in grain morphology and size while chemical composition remains relatively constant [20].

2.4. pH studies

Coating composition and quality is dependent on the pH of the system at the time of formation. Although extensive work has been done on zinc-nickel coatings in both acidic and alkaline conditions, less work has been done on zinc-nickel coatings with nanoparticle incorporation. A review of the literature shows most studies being performed under acidic conditions [32–37, 39–40, 44, 46] with little work in alkaline conditions [12, 42, 48]. ZnNi-Al_2O_3 coatings were predominantly deposited under acidic conditions (pH = 4, 4.9 and 5.0) with one group examining deposition at pH = 13 [12, 27–33]. The literature for the deposition of ZnNi-TiO_2 coatings was done under acidic conditions with pH = 2.5, 4 and 4.6 from a variety of groups [11, 34–37]. The deposition of ZnNi-SiO_2 particles was performed at pH = 2, 3 and 4 while the deposition of ZnNi-SiC was done under an unspecified alkaline pH [26, 38, 39–42]. The deposition of ZnNi-ceria particles was undertaken with a pH = 5.3 [43, 44]. ZnNi-carbon nanotubes, though not specified are believed to have been deposited under alkaline conditions due to specified bath components [13, 45] and the deposition of ZnNi-Mt coatings was done at pH = 9.4 [48]. Though the bulk of the work has been done under acidic conditions, focus of the research may benefit from pushing into the realm of alkaline deposition as throughout literature, optimal coating formation is realized under alkaline conditions. Although zinc-nickel coatings deposited under acidic conditions tend to have a higher current efficiency, alkaline processes tend to lead to better substrate coverage [12, 57, 62, 79]. A drawback of alkaline conditions is stabilizing agents are needed to keep the metal species from precipitating as metal hydroxides from the solution.

3. Characterization of the zinc-nickel nanocomposite coatings

3.1. Coating composition

Zinc and nickel content and nanoparticle incorporation were examined with various techniques including atomic absorption spectroscopy (AAS), inductively coupled plasma-mass spectrometry (ICP-MS), energy dispersive spectroscopy (EDS) energy dispersive x-ray (EDX) and EDX mapping. Uptake of the nanoparticles is of interest as varying concentrations of nanoparticles are found, dependent upon the character of the particle being added to the solution. ZnNi coatings with Al_2O_3 incorporation were found to contain anywhere from trace Al_2O_3 up to 8.9 wt % throughout the literature [12, 27–33]. Zinc-nickel coatings with TiO_2 incorporation were found to contain on average 80–85% Zn, 12–17% Ni and 1.25–2.5% Ti [35–37]. ZnNi-SiC coatings contained 11% SiC [42]. ZnNi coatings with ceria incorporation contained 10–11% Ni, with 2–3% ceria content [43, 44]. ZnNi-Mt coatings contained 86–90% Zn, 10–14% Ni with trace amounts of Mg and Al from Mt nanoparticles confirmed in ICP-MS analysis [48]. Throughout the studies, the coatings maintain the Ni% needed (8–18%) for maximized corrosion protection [57, 59, 70, 83].

3.2. X-ray diffraction (XRD)

The phase of electrodeposited ZnNi alloy coatings is dependent upon the nickel content in the alloy and can be controlled by a number of factors including electrolytic bath conditions [12]. ΥNi_5Zn_{21} is known to be the most corrosion resistant ZnNi alloy phase and appears to be preferentially deposited under alkaline conditions in ZnNi systems without nanoparticle incorporation. The γ ZnNi has a preferred orientation with the (330) reflection as main peak in the XRD pattern [42, 59, 65–67, 71, 72]. This preferred orientation continues with the incorporation of nanoparticles although an overall decrease in peak intensity and broadening of peak suggest smaller crystallite size formation [12, 35, 48]. The peak width of the diffraction peak at half maximum height (FWHM) is dependent on crystallite size and lattice strains due to lattice imperfections such as dislocations or atom vacancies with the values dependent most heavily on crystallite size [84, 85]. If we assume there is little strain in the system, we can assume the broadening at FWHM is due to a decrease in crystallite size of the metallic particles [35]. The average crystallite size of ZnNi coatings with TiO_2, SiC, and Al_2O_3 nanoparticles are presented in **Table 2**. The trends show an overall decrease in particle size with the increase in nanoparticle incorporation as compared to pure ZnNi coatings.

3.3. Microhardness

Hardness (HV) values are a measurement of the microhardness or resistance to penetration of a sample and can be used to compare quality of the coatings. All composite coatings studied demonstrate improved microhardness values as compared to the base alloy as presented in **Table 3**. As expected, addition of nanoparticles to the coatings improve the overall hardness values, as demonstrated with an increase of 305 HV to 524 HV for ZnNi coatings with CeO_2 treated SiO_2 particles, an increase of 35 HV with the addition of TiO_2 particles in Praveen's work, a 300% increase in hardness with an incorporation of 11.2 wt % Al_2O_3 particles in Zheng's work and noticeable increases in both Ataie's and Ghaziof's work with incorporation of Al_2O_3 particles as well [27, 29, 32, 37, 47]. The improved microhardness is believed to be due to dispersive strengthening as the ceramic like particles (TiO_2) form a barrier to deformation commonly observed in metal matrix systems. As the incorporation of nanoparticles increases, the microhardness also increases [36]. The higher hardness of the coating is due to the fine-grained structure. The dispersed particles in the matrix are able to obstruct easy movement of dislocations [37].

Nanoparticle	ZnNi (nm)	ZnNi nanocomposite (nm)
Al_2O_3 (5 g/L) [17]	40.93	26.4
Al_2O_3 (10 g/L) [17]	40.93	33.2
Al_2O_3 (15 g/L) [17]	40.93	20.68
TiO_2 [43]	—	30
TiO_2 [41]	—	19.7
TiO_2 [40]	15.5	11.7
SiC [48]	28.5	21.0–22.0

Table 2. Crystallite size of coatings listed in the literature.

Reference	Coating composition	Hardness values (HV)	Additional parameters
Xiang et al. [53]	Bare substrate	134	Direct deposition
	ZnNi coating	305	
	ZnNi coating with incorporated SiO_2 nanoparticles	535	
	ZnNi coating with incorporated CeO_2 treated, SiO_2 nanoparticles	524	
Ataie et al. [35]	ZnNi Coating with incorporated Al_2O_3 nanoparticles	340	Direct deposition
	ZnNi Coating with incorporated Al_2O_3 nanoparticles	640	30 W ultrasonic application during deposition
	ZnNi Coating with incorporated Al_2O_3 nanoparticles	750	45 W ultrasonic application during deposition
Zheng et al. [38]	ZnNi coating	215	Ultrasound generation and magnetic stirring during deposition
	ZnNi coating with incorporated 11.2 wt % Al_2O_3 nanoparticles	640	
Praveen et al. [43]	Zinc-nickel coating	135	Direct deposition
	ZnNi with incorporated TiO_2 particles	170	
Ghaziof et al. [33]	ZnNi coating with incorporated Al_2O_3 nanoparticles	235	Direct deposition
	ZnNi coating with incorporated Al_2O_3 nanoparticles	310	Pulsed current deposition, 100 Hz
	ZnNi coating with incorporated Al_2O_3 nanoparticles	323	Pulsed current deposition, 500 Hz

Table 3. Microhardness values of coatings throughout the literature.

3.4. Corrosion studies

An advantage to developing metal matrix composite coatings is for increased corrosion resistance as compared to pure metal coatings. Properties that may contribute to this added protection include a finer coating structure with refined grains, incorporation of electrochemically inert particles dispersed throughout the metallic coating, and filling of crevices, gaps, and micron sized holes on the coatings surface. These could otherwise lead to localized defects which are vulnerable to corrosion. Improvement of self-passivation of the coating is offered through improved barrier protection due to the incorporated particles in the naturally formed defects of the coatings. Common methods to examine the corrosion resistance of a material include open circuit potential (OCP) studies, linear polarization resistance (LPR), potentiodynamic polarization, and electrochemical impedance spectroscopy (EIS).

The open circuit potential (OCP) is the potential of the working electrode relative to the reference electrode when no external potential or current is being applied to the system. OCP is dependent on the composition of the working electrode, treatment of the electrode prior

to the study, and the electrolytic bath in which the electrode resides. Linear polarization resistance is the measurement of current in relation to the electrode potential. This can be used to predict the corrosion rate of the coatings within a specific environment. The film is polarized by applying an external potential forcing the system away from equilibrium and monitoring the resulting potential and current. The deviation from an equilibrium potential is called polarization. The polarization resistance (R_p) is experimentally observed between the electrochemical current density and applied potential for the corroding electrode within a few millivolts of the polarization from the open circuit potential (E_{ocp}). Potentiodynamic polarization pushes the potential even further from the equilibrium potential for the anodic and cathodic sweeps. From this data the anodic slope (β_a) and cathodic slope (β_c) are obtained from the curves. The E_{corr} is determined from the intercepts of the curves. The i_{corr} value is obtained by substituting the β_a, β_c and R_p values into a simplified rearranged Stern and Geary equation [86, 87].

The anticorrosive ability of ZnNi-nanocomposite coatings can be further investigated with EIS. Nyquist plots show a semicircle shape in the investigated frequency range with an increased axial radius, which is indicative of better corrosion resistance. Equivalent circuit models are used to simulate the metal-solution interface to better understand the system. A few studies have done corrosion work for these ZnNi nanocomposite coatings and shown improvement with addition of the nanoparticles. **Table 4** lists some results which are discussed in sections below.

Coating [ref]	E_{corr} (V)/SCE	i_{corr} (A)	R_p (Ω cm^2)
Zn [54]	−1.17	2.09×10^{-4}	1333
Ni	−0.45	2.75×10^{-5}	6790
ZnNi γ phase	−0.74	1.06×10^{-5}	30,485
ZnNi-Mt γ phase	−0.73	3.72×10^{-6}	34,900
ZnNi [50]	−0.92	6.20×10^{-5}	—
ZnNi-CeO_2	−0.77	3.30×10^{-5}	—
ZnNi-CeO_2 (sonicated)	−0.78	2.80×10^{-5}	—
ZnNi-TiO_2 [41]	−1.09*	9.90×10^{-5}	122.2
ZnNi	−1.05*	4.30×10^{-5}	352.0
ZnNi-TiO_2 (24 h immersion)	−1.11*	1.25×10^{-5}	97.3
ZnNi (24 h immersion)	−1.03*	—	94.1
ZnNi [17]	−0.62	2.51×10^{-6}	1167.6
ZnNi-Al_2O_3 5 g/L	−0.52	1.23×10^{-6}	4024.9
ZnNi-Al_2O_3 10 g/L	−0.63	2.37×10^{-6}	2038.3
ZnNi-Al_2O_3 15 g/L	−0.70	2.57×10^{-6}	1190.0

*Corrected to SCE.

Table 4. Corrosion potential (E_{corr}), corrosion current (i_{corr}) and polarization resistance (R_p) of ZnNi and ZnNi-Mt coatings.

4. Zinc-nickel nanocomposites

4.1. ZnNi-Al_2O_3 and Al_2O_3/SiC

Most work to date has examined ZnNi-Al_2O_3 coatings (~32% of papers) with 4% examining the effects of Al_2O_2/SiC combined in the nanocomposite. Though the deposition mechanism of ZnNi-Al_2O_3 coatings was not explicitly discussed, Tulio et al. examined the effects of SiC and Al_2O_3 in slightly acidic pH with rotating disc. They first examined the effect of SiC and Al_2O_3 on nickel and zinc, without the other metal ion present in solution and found the addition of SiC and Al_2O_3 encouraged deposition of both Ni and Zn individually. For nickel, a marked increase in current densities was observed. In the Zn system when the solution was scanned cathodically without the presence of nanoparticles, the deposit exhibited many discontinuities, or areas without a deposit present. When the SiC and Al_2O_3 particles were added to the solution, there was a noticeable increase of coating coverage so much that the discontinuities almost disappeared entirely, suggesting encouragement of Zn deposition. SiC and Al_2O_3 do not affect the initial nucleation and growth in the ZnNi system when the metal species are combined, though at higher concentrations of nanoparticles, surface blockage has been observed. Larger current densities are observed for systems with SiC and Al_2O_3 as compared to systems free of nanoparticle presence and a positive shift in potential was noted at the onset of secondary nucleation. This is due to an increase in the mass-transport of the particles to the electrode surface during the rotation. During the scans the quantity of particles reaching the electrode increased, leading to an increase in current density. The ZnNi deposition did remain anomalous under all conditions examined [46]. Blejan and Muresan examined the XRD patterns of deposited ZnNi-Al_2O_3 films (using a Cr x-ray tube), which only exhibited γ-phase ZnNi alloys, showing small growth of the (330) plane with addition of Al_2O_3 particles with deposition giving a preferred (600) orientation [12]. Improvement of nanoparticle incorporation was noted through the use of ultrasonication [29, 32, 33].

Zhang and An found an increase of hardness with the addition of Al_2O_3 [32]. Ataie et al. examined the effect of sonication during the deposition. Without sonication, the hardness was 340 HV, with 30 W sonication it was 640 HV and with 45 W sonication it was 750, a 220% increase over the coating with no sonication [29]. The hardness of ZnNi and ZnNi-Al_2O_3 coatings under direct current and pulse current deposition conditions was examined. ZnNi under applied current was 235 HV while pulsed ZnNi was 310–323 HV, a 40% increase and ZnNi-Al_2O_3 was 338 HV, a slight increase over pulsed ZnNi coatings [27]. Shourgeshty et al. examined multilayer coatings of ZnNi and ZnNi-Al_2O_3 deposits. As expected, an increase in the number of layers improved the hardness values of the coatings but addition of Al_2O_3 also had a positive effect [30, 31].

ZnNi-Al_2O_3 coatings were studied in Na_2SO_4 solution. ZnNi-Al_2O_3 coatings (**Table 4**) present corrosion potentials of the composite coatings at more positive potential with initial Al_2O_3 incorporation as compared to ZnNi alloys which is attributed to the chemical inertia of the incorporated particles [12]. The corrosion current decreases from 1.83×10^{-5} to 0.92×10^{-5} as the Al_2O_3 content is doubled from 4.5 to 8.9 wt% [32]. EIS of ZnNi-Al_2O_3 with varying incorporation

of Al_2O_3 and varying immersion (0, 24, 48 and 120 h) is presented in **Figure 2**. The coatings were studied in 0.2 g/L Na_2SO_4 (pH 5) using a potentiostat PARStat 2273 (Princeton Applied Research). The frequency domain was 10 kHz to 100 mHz and temperature was maintained at 23 ± 2°C. The plots were fit with ZSimpWin 3.21 software. The impedance modulus of the nanocomposite is higher than pure ZnNi films. The charge transfer resistance for the composite coating is higher than ZnNi films, yet the double layer capacitance is smaller. Initially the measurement decreases at a systematic rate, suggesting a rapid degradation of the coating due to corrosion but after 50 h the rate of degradation decreases, likely due to the formation of corrosion products on the surface of the coating [12]. Incorporation of Al_2O_3 particles results in γ-phase zinc-nickel alloys with nanoparticle incorporation. ZnNi-Al_2O_3/SiC coatings still follow an anomalous deposition route. Improved hardness and corrosion properties are observed with incorporation of Al_2O_3 [12, 27, 29, 32, 46].

4.2. ZnNi-TiO_2

ZnNi-TiO_2 coatings comprise ~20% of the papers on ZnNi-nanocomposite coatings. As demonstrated with the Al_2O_3 composite coatings, improved corrosion and mechanical properties of the ZnNi coatings occur with the incorporation of TiO_2 particles into the metal matrix. In a study by Praveen et al. they varied the TiO_2 concentration in the bath from 0.5 to 5.0 g/L. Lower current densities were observed at 3 g/L and above this concentration the corrosion current increased so it was chosen as the optimal concentration [37].

The deposition with TiO_2 gave coatings with preferential γ-phase alloy, though small amounts of a pure zinc phase are seen in ZnNi coatings without TiO_2 incorporation. Textural modifications due to the presence of TiO_2 nanoparticles are suggested due to slight changes in peak intensity in the XRD patterns as compared to ZnNi coatings without TiO_2 incorporation. The metallic grain size also decreases with the incorporation of TiO_2, due to changes to nucleation and growth due to disruption of the metallic growth by incorporation of semiconducting particles during coating formation [35]. TiO_2 incorporation can also cause a considerable decrease in grain size for the metallic phase, with rough and irregular deposits as demonstrated by SEM and AFM (**Figure 3**) [34, 35]. The ZnNi coating without TiO_2 exhibited multiple defects, cracks, gaps, crevices and microholes. The TiO_2 nanoparticles fill these gaps, leading to an overall decrease in the corrosion rate. The crystal size of the composite coating also appears smaller as compared to the ZnNi coating [37]. The compact size is preferred as it also better protects from corrosion onset. The effects of soniciaton on morphology were also examined. Ultrasonic vibration during deposition was found to result in increased nanoaparticle incorporation and a more homogeneous coating, suggesting the vibration promotes uniform distribution of the particles and decreased agglomeration of the particles. Improvement of nanoparticle incorporation due to ultrasonicaiton was also noted [36].

TiO_2 particles restrained the growth of the ZnNi alloy grains leading to a significantly higher microhardness in the presence of TiO_2 [37]. As expected, with increasing nanoparticle incorporation, the hardness increases, which is believed to be due to the dispersion of the ceramic like TiO_2 particles throughout the metal matrix [36]. As observed with Al_2O_3 addition, sonication of the electrolytic bath lead to increased microparticle incorporation, with hardness

http://dx.doi.org/10.5772/intechopen.80219

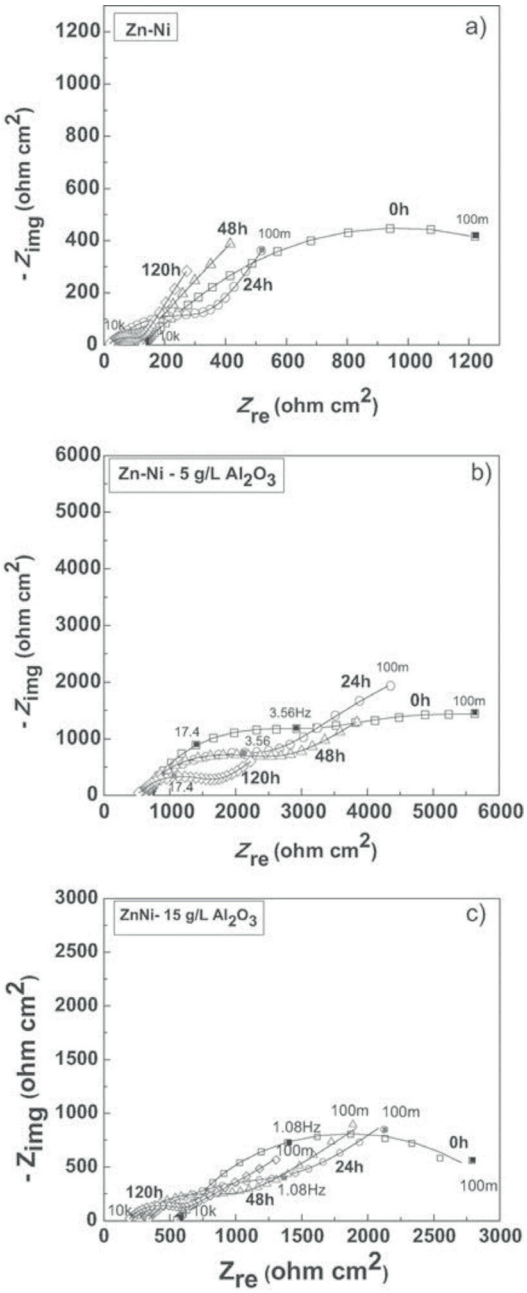


Figure 2. Impedance spectra of electrodeposited ZnNi and ZnNi-Al_2O_3 coatings, a) ZnNi, b) ZnNi-5 g/L Al_2O_3 and c) ZnNi-15 g/L Al_2O_3, recorded at 0, 24, 48 and 120 h immersion in 0.2 g/L Na_2SO_4 solution. "Reprinted with permission from [17]. Copyright 2013, John Wiley and Sons."

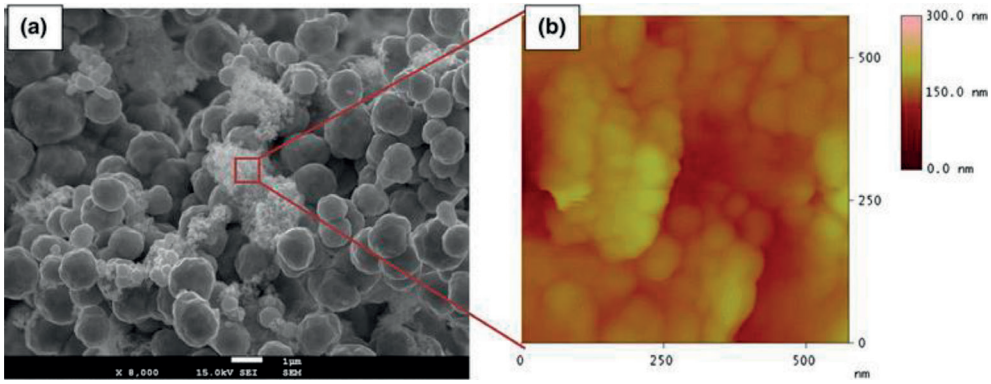


Figure 3. Morphology of ZnNi-TiO_2 coatings (a) SEM and (b) AFM. "Reprinted with permission from [41]. Copyright 2012, Springer Nature."

increasing from 253 HV for ZnNi coatings, and 464 for ZnNi-TiO_2 coatings without sonication, to 754 HV for ZnNi TiO_2 with sonication during deposition, a 60% increase in hardness with sonication and a 200% increase in hardness as compared to coating with the addition of Al_2O_3 particles incorporated under sonication. TiO_2 particles hinder the dislocation of movement, leading to an increased hardness of the material though a reverse trend which was observed at higher concentrations of TiO_2 in the deposition bath and believed to be due to agglomeration of the nanoparticles in solution [37].

The OCP was monitored over time for ZnNi and ZnNi-TiO_2 coatings in 3.5% NaCl and near-neutral 0.05 M Na_2SO_4 solutions, respectively [35]. The initial OCP values show that OCP of ZnNi and ZnNi-TiO_2 coatings appear at more noble values due to the presence of nickel (a more noble metal as compared to zinc) in the coating. Initially, the OCP values were − 1.49, −1.51, −1.43 and − 1.23 V (vs. Hg/Hg_2SO_4) for Zn, Zn-TiO_2, ZnNi and ZnNi-TiO_2, respectfully. After 24 h submersion, these values changed to −1.47, −1.49, −1.18 and −1.10 V for Zn, Zn-TiO_2, ZnNi and ZnNi-TiO_2, respectfully. The ZnNi coating undergoes the most drastic change in OCP in the 24 h time frame. The ZnNi-TiO_2 appears to reach a steady state at a faster rate than ZnNi, possibly due to the smaller grain size of the particles due to nanoparticle incorporation [35]. There is a small positive shift in all coatings, due to dissolution of zinc on the surface of the coating, as zinc undergoes a sacrificial protection method.

The polarization of ZnNi and ZnNi-TiO_2 coatings were found to have a larger corrosion current after 24 h of submersion in 0.05 M Na_2SO_4 solution than the as deposited coatings but the ZnNi-TiO_2 coating still maintained a smaller corrosion current value than the ZnNi coating even after immersion (**Table 4**). The microstructure of as deposited and submerged coatings was examined to determine any structural design which could affect the corrosion current of each coating. The incorporation of TiO_2 nanoparticles decreased the grain size of the metallic phase and the coatings appear more rough and irregular in surface morphology [35]. The initial increase in corrosion current observed by ZnNi-TiO_2 coatings prior to submersion are attributed to the smaller grain size and more porous structure observed in the coatings. The higher porosity of the coatings could be the cause of the increased corrosion resistance [34, 35]. Polarization curves and kinetic data show ZnNi-TiO_2 and ZnNi deposits initially have a high

corrosion density (0.4–0.6 mA/cm^2) and low polarization resistance. At 24 h immersion in the Na_2SO_4 solution, the i_{corr} of the ZnNi-TiO_2 coating has decreased by a factor of 5 and the R_p had increased by a factor of 3. The ZnNi-TiO_2 coating presented the highest corrosion protection after 24 h immersion [35]. ZnNi-TiO_2 coatings were examined in 3.5% NaCl solution and a decrease in corrosion current density was observed as TiO_2 was incorporated into the coating, with a decreasing trend following increased sonication of the particles prior to deposition [36]. Coatings throughout literature demonstrate a wide array of corrosion potentials, varying from E = −0.5 to −1.2 V, which follow values found for ZnNi coatings [12, 28, 30–32, 34–37, 39, 43, 44]. The value of the corrosion potential, which can show corrosion tendencies, is indicative of the components of the coatings. The optimal corrosion potential will lie between that of a pure zinc coating and a pure nickel coating, as it will have character of each metal and with that, corrosion behavior of each metal. The corrosion current, which is proportional to the corrosion rate, does decrease with the incorporation of nanoparticles as demonstrated in **Table 4**. The addition of nanoparticles, even in small amounts shows an overall improvement on the corrosion potential, corrosion current and resistivity of the systems.

Momeni et al. studied ZnNi-TiO_2 coatings on copper substrates as a possible coating for antibacterial inhibition, specifically the antibacterial resistance toward Gram positive (*Staphylococcus aureus* PTCC1431) and Gram negative (*E. coli* PTCC1394) bacteria through an inhibition zone method (**Figure 4**). The bacterial strains were transferred into flasks containing nutrient broth and bacteria which had been cultured at 37°C under aerated conditions. An agar diffusion test was used to study antibacterial activity. Inoculums of *E. coli* and *S. aureus* were spread over the surface of the nutrient agar, and the ZnNi-TiO_2 sample was placed

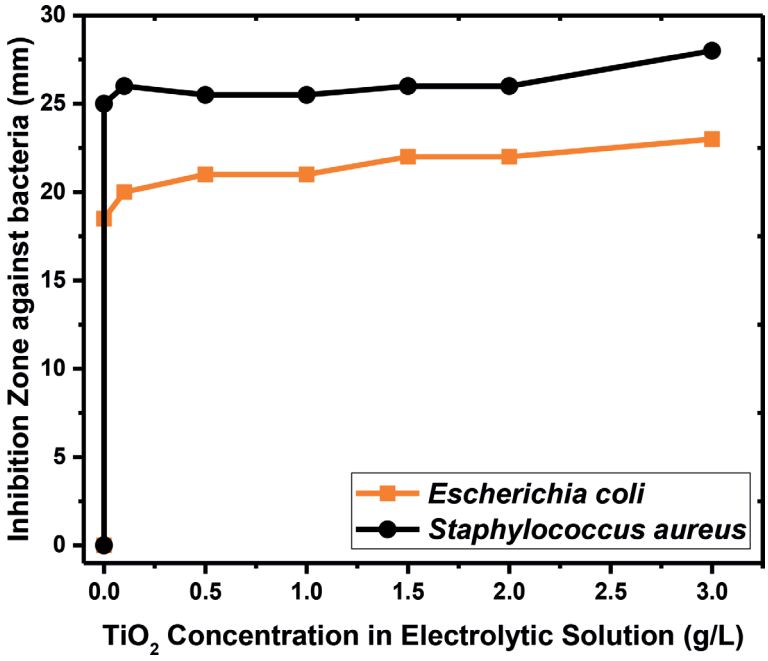


Figure 4. Inhibition capability of ZnNi-TiO_2 coatings with increase of TiO_2 in the electrolytic bath [14].

onto this sample and incubated for 24 h at 37°C. The best coating was found to be ZnNi-TiO_2 prepared with 3 g/L TiO_2 in solution, which had an inhibition zone of 23 mm for *E. coli* and 28 mm for *S. aureus* [11].

4.3. ZnNi-SiO_2 and ZnNi-SiC

SiO_2 and SiC comprise ~20% of the literature on ZnNi-nanocomposite coatings. SiO_2 was examined by Tuaweri and Wilcox. They studied the change in current density as a function of % Ni in the deposit with and without bath agitation, and with varying SiO_2 particle size. SiO_2 is believed to deposit with the ZnNi coating under a codeposition mechanism. As expected, without SiO_2 presence in the bath, nickel appears to follow an anomalous deposition mechanism as the current density of the system is increased from 3 to 6 A/dm^2. When 26 g/L of 20 nm SiO_2 particles was added to the system, a transition from anomalous to normal deposition is noted at 4 A/dm^2 [38]. The SiO_2 colloids have been previously noted to increase deposition rate of Fe group metals [40]. SiO_2 colloids shift this deposition from an anomalous mechanism to a normal mechanism. A possible explanation is due to adsorption of the Fe group metals onto the SiO_2 nanoparticles in the electrolytic bath. During the deposition process, the pH of the electrolyte at the working electrode surface increases, or becomes more alkaline due to removal of hydrogen by the generation of hydrogen gas, also known as hydrogen evolution. The SiO_2 particles tend to agglomerate once a neutral pH is reached, so the agglomerated colloid can suppress $Zn(OH)_2$ formation causing a slowing in the diffusion of zinc ions from the solution, through the inner layer and to the cathode for reduction. As the SiO_2 particle size was increased from 20 nm to 2 μm, a slightly higher nickel wt. % was observed in the coatings. Addition of the SiO_2 nanoparticles resulted in increased Ni wt. % at all current densities, as compared to coatings without SiO_2. This suggests that the SiO_2 in the bath encourages the deposition of nickel in the coating. Throughout the studies SiO_2 appears to have an overall effect on the deposition mechanism of ZnNi coatings through emergence of a normal deposition route, while SiC continues to follow an anomalous deposition pattern. Further studies need to be completed in this area to determine if increased particle presence will encourage a transition from anomalous to normal deposition for other systems or if this is unique to the behavior of SiO_2 nanoparticles in the ZnNi electrolytic system.

Tuaweri et al. found the corrosion potentials of ZnNi and ZnNi-SiO_2 coatings were more anodic as compared to zinc. Under open circuit potential conditions, ZnNi and ZnNi-SiO_2 coatings behave in a similar manner, but once the applied potential is increased, the ZnNi-SiO_2 coatings shift toward more anodic potentials as compared to ZnNi coatings. This suggests the presence of SiO_2 promoted shifting of the dissolution potential to more anodic values as compared to ZnNi due to the inert nature of SiO_2 particles and possible changes in the deposition mechanism in the presence of SiO_2. SiO_2 appears to have an overall effect on properties such as deposit texture, morphology, microstructure due to the ability of the SiO_2 particles to provide barrier protection to the coating through packing of microholes, gaps and crevices in the coating [38]. The incorporation of SiC and SiO_2 nanoparticles shows no changes on phase composition, with γ-phase being the predominant phase in the XRD patterns. Some Zn_{101}, Zn_{102} and δ-phase XRD peaks were observed, but this was expected as these coatings were deposited under acidic conditions. Low intensity peaks corresponding to SiO_2 confirms incorporation of the nanoparticles into the coatings without leading to any structural phase changes [39, 42].

In other nanoparticle coatings, we find similar trends such as finely grained, uniform, clearly pronounced crystal structures with the incorporation of SiO_2 and SiC [26, 38, 40, 41]. Finer grains were common with even distribution of the nanoparticle in the coatings [42]. SiO_2 coatings were examined for hardness changes, and showed an increase in hardness with an increase in current density during deposition of the coatings. Coatings were deposited from 2.0–5.0 A/dm^2 in increments of 1, and hardness values increased correspondingly from 155 to 210 HV. The improved hardness of the coating was attributed to the incorporation of SiO_2 particles which add mechanical strength due to embedded SiO_2 particles [39].

4.4. ZnNi-CeO_2 and SiO_2/CeO_2

ZnNi-CeO_2 coatings comprise ~8% of the literature, while ZnNi-SiO_2/CeO_2 comprises ~4%. Nanoparticle incorporation was found to be improved through pulsed deposition methods [43, 44]. Exbrayat et al. examined ZnNi coatings with ceria incorporation and confirmed the presence of single phase γ Ni_5Zn_{21} with preference to the (330) plane as previously observed in other deposition systems. The intensity of the (600) reflection increases with the addition of ceria particles, which could be attributed to the preferential incorporation of ceria nanoparticles at the grain boundaries which affects the overall growth of the crystals [44]. The incorporation of CeO_2 nanoparticles is shown in **Figure 5** for the SEM micrographs. Ceria nanoparticles were first added to the electrolytic bath without prior sonication (**Figure 5a**), and the nanoparticles agglomerated into long string-shape structures. Due to the agglomeration tendancies of the nanoparticles, sonication of the nanoparticles prior to depositon was examined. The coatings obtained from the sample post sonication (**Figure 5b**) take on a pyramidal growth pattern and appear more coarse. EDX was used to determine placement of the nanoparticles in the coating and the CeO_2 particles appear to be primarily adsorbed onto the electrode surface. The agglomerated nanoparticles appear uniformly trapped inside the metal matrix. Ultrasonic agitation was done at 20°C with an amplitude value of 35 (power of 41 W/cm^2, output frequency of 20 kHz) for 20 min prior to deposition. As the samples were sonicated prior to deposition, the agglomerated particles dispersed and were able to better fill the voids and pores naturally formed in the matrix, leading to better overall corrosion protection [43, 44]. Improvement of nanoparticle incorporation through the use of ultrasonication, previously noted for other systems including TiO_2 and Al_2O_3 was also noted for CeO_2 [32, 33, 36, 43, 44].

The OCP of ZnNi-CeO_2 coatings was measured in 3.5% NaCl and near-neutral 0.05 M Na_2SO_4 solutions, respectively and monitored over time [44]. Exbrayat et al. studied two differing ZnNi-CeO_2 samples, ZnNi-CeO_2 which was determined to contain 84% Zn, 14% Ni and 2% CeO_2 and ZnNi-Ce_2 (sonicated) which was found to contain 85% Zn, 12.8% Ni and 2.2% CeO_2. When first submerged in the Na_2SO_4 solution, the OCP values changed drastically for ZnNi, ZnNi-CeO_2 and ZnNi-CeO_2 (sonicated). For ZnNi, a significant ennoblement was observed moving from an OCP value more cathodic than E = −0.95 V to E = −0.55 V after ~20 h of submersion. The OCP then begins to decrease steadily before stabilizing at ~E = −0.65 V after 96 h of immersion. ZnNi-CeO_2 (sonicated) follows a similar pattern to ZnNi, with a shift in OCP from ~E = −0.85 V initially to ~−0.57 V after 30 h of submersion, while ZnNi-CeO_2 which was not sonicated prior to deposition, stayed relatively stable throughout the 4 day submersion test, decreasing in OCP from ~E = −0.82 V to ~E = −0.75 V. Zinc coatings often settle

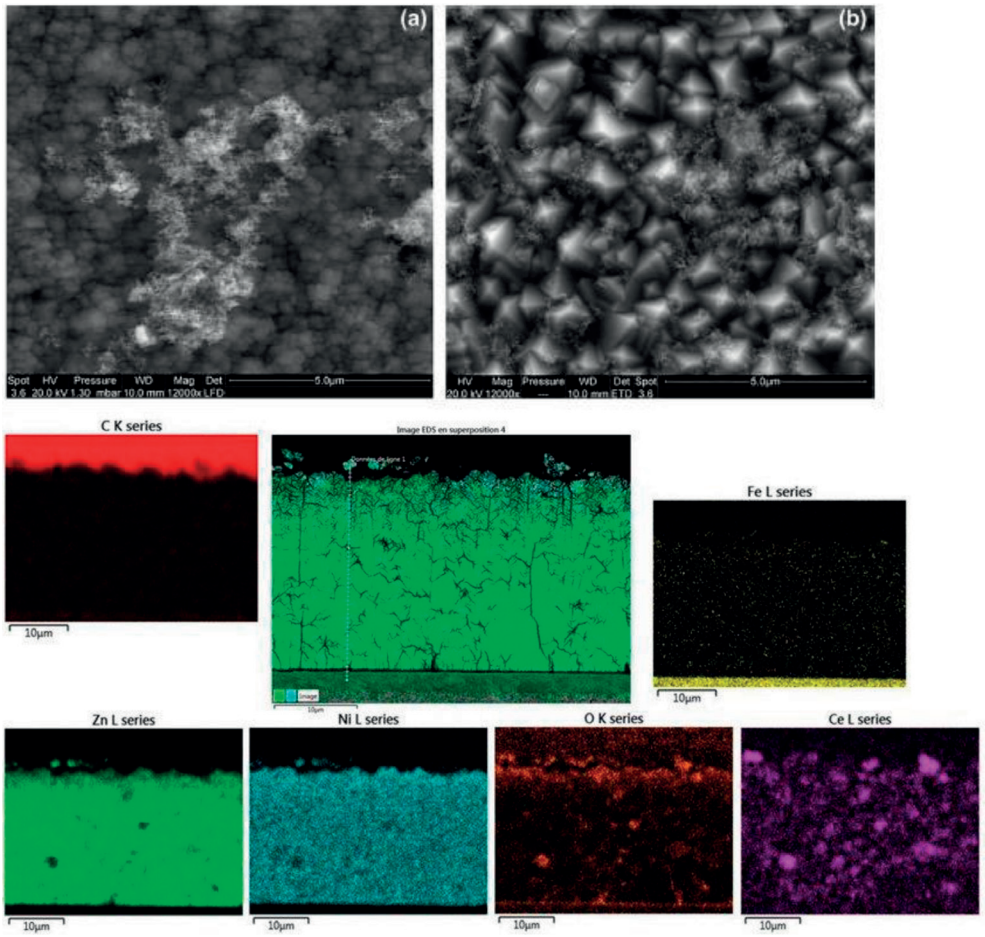


Figure 5. SEM micrographs of electrodeposited ZnNi-CeO_2 nanoparticle coatings without prior sonication (a) and with prior sonication (b), and X-ray maps of the main elements in the coating. "Reprinted with permission from [50]. Copyright [2017], John Wiley and Sons."

over the initial submersion due to the formation of corrosion products, which then begin to protect the coating [43, 44]. EIS of ZnNi-CeO_2 coatings were examined using a PGP 301 Autolab potentiostat after 24, 48, 96 h immersion in 35 g/L saline solution at 25°C with a frequency range of 64 kHz to 1 mHz, AC voltage amplitude of ±10 mV. Analysis was completed with Zview software. The Nyquist diagrams exhibit two capacitive loops at middle and low frequencies, with similar time constants. The loop diameter of the ZnNi coating remains relatively constant, suggesting stability in the corrosion rate. In the nanocomposite coatings, the loop diameter increased with immersion time. The incorporation of ceria enhances the corrosion resistance by ennoblement of the surface through reduction of galvanic corrosion of the steel [44].

4.5. ZnNi-carbon nanotubes

ZnNi-carbon nanotubes comprise ~8% of the literature to date. The dispersion, linear sweep voltammetry, surface morphology and friction properties of ZnNi coatings with nanotube incorporation was discussed. When carbon nanotubes were introduced into a ZnNi electrolytic solution, a positive shift (~0.1 V) in the polarization curves were observed and the deposition current of the system increased. The transport of the carbon nanotubes to the cathode surface and their incorporation into the coating is believed to be due to adsorption of Zn^{2+} and Ni^{2+} ions onto the nanotubes which are then reduced onto the coating, thereby entrapping the nanotubes in the coating. Initially the nanoparticles are weakly adsorbed onto the cathode, but once the particles lose their ionic and solvation shells, they become securely attached to the surface of the deposit. The adsorbed metal ions on the surface of the dispersed phase discharge at this point permanently attaching the nanotube to the coating [13, 45]. The actual deposition mechanism is not discussed in this work, so it is unclear if the nanotubes have an overall effect on the deposition mechanism or if anomalous deposition is still followed for this system.

In the case of carbon nanotubes, they are believed to act as nuclei for crystallization, further promoting even distribution of the nanotubes throughout the cathode surface. Microcracks are often observed in ZnNi coatings, but once carbon nanotubes have been added to the electrolytic mixture, the surface appears uniform and dense.

Another property examined for ZnNi-carbon nanotube nanocomposites was the sliding friction coefficient of the coatings as compared to ZnNi coatings. The ZnNi-carbon nanotube coatings were found to have a sliding friction coefficient 1.3–1.5 times smaller than ZnNi coatings without nanotube disbursement both in direct current and reverse current deposition modes. ZnNi coatings showed a decrease in friction coefficient values from 0.30 to 0.24 for current densities changing from 1.0 to 2.5 (A/dm^2) while the corresponding ZnNi-carbon nanotube coatings decreased from 0.23 to 0.17 for the same current density values. Under a reverse current mode, ZnNi coatings had friction coefficients starting at 0.31 and decreasing to 0.23 as the ratio between cathodic and anodic periods was increased from 10:1 to 16:1 while for ZnNi-carbon nanotube coatings under the same conditions, the friction coefficients decreased from 0.24 to 0.15 [13, 45].

4.6. ZnNi-Mt

The effect of montmorillonite (Mt) addition to the ZnNi bath was examined through anodic linear sweep voltammetry (ALSV) as presented in **Figure 6**. Montmorillonite is a smectite mineral and has a 2:1 layered structure, with two layers of silicon tetrahedral sandwiching one layer of aluminum octahedral. The layers can be stacked together, but when the van der Waals forces holding the individual clay layers together are overwhelmed, the individual layers become exfoliated (also known as delaminated). For this work, mechanical agitation and/or sonication was used to exfoliate the layered silicate and produce individual nanoplatelets. Individual montmorillonite nanoplatelets exist as coordinated layers, measuring 1–2 nm thick. Mt is a hydrous aluminum silicate with approximate formula (Na,Ca) $(Al, Mg)_6(Si_4O_{10})_3$-$(OH)_6.nH_2O$. The Al^{3+} and Si^{4+} locations can be replaced by lower valent cations, causing the montmorillonite structure to have an excess of electrons. The negative

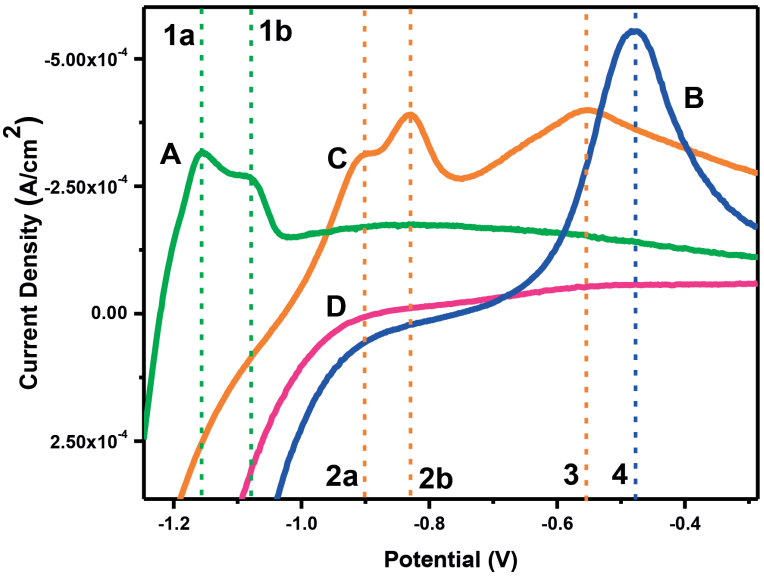


Figure 6. Anodic linear sweep voltammetry (ALSV) data of 1:1 molar ratio equivalent of $ZnSO_4{\cdot}H_2O$: $Ni(NH_4)_2(SO_4)_2{\cdot}6H_2O$ all solutions prepared in 0.1 g/100 mL Mt in 0.1 M borate solution, pH = 9.40 with NH_4OH, sweep rate of 50 mV/S. (A) Zn^{2+}; (B) Ni^{2+}; (C) Zn^{2+} and Ni^{2+}; (D) no Zn^{2+} or Ni^{2+} present; (1a, 1b) anodic stripping potentials of Zn^{2+}; (2a, 2b) anodic stripping potentials of Zn^{2+} in presence of Ni^{2+}; (3) anodic stripping potential Ni^{2+} in presence of Zn^{2+}; (4) Ni^{2+} anodic stripping potential [54].

charge is compensated through loosely held cations from the associated water. Sodium montmorillonite, the clay mineral in which the loosely held cation is the Na^+ ion, was the clay source used throughout the work. ALSV was used to obtain initial dissolution data of Zn^{2+} and Ni^{2+} ions in solution, as well as any electrochemical effect of the Mt nanoparticles on the metal dissolution peaks and the electrochemical behavior of Mt. The potential was scanned from OCP to E = −1.5 V (vs. SCE) at a sweep rate of 50 mV/s, held briefly and scanned back to OCP. During the anodic scan, the metals of interest were stripped back into the electrolytic solution. As previously observed for zinc-nickel systems under anomalous deposition control [57, 62, 69, 79], the anodic stripping peaks of the metals in solution are shifted based on other metal species in solution. According to the linear sweep voltammetry (LSV) data, zinc in the electrolytic solution had two anodic dissolution peaks present at potentials of E = −1.12 V and E = −1.08 V. During the cathodic scan, a small $Zn(OH)_2$ layer deposits on the steel surface, slowing down dissolution kinetics. The dissolution of this species caused the second peak in the LSV [48, 57, 88]. Nickel had an anodic dissolution peak present at a potential of E = −0.48 V. When combined in solution, the zinc anodic dissolution peaks were shifted to potentials of E = −0.91 V, E = −0.83 V and the nickel anodic dissolution peak was shifted to a potential of E = −0.55 V. As previously stated, the zinc-nickel dissolution peaks of zinc and nickel are shifted in potential with respect to the individual metals in solution and this is indicative of an anomalous deposition system [51, 70, 76]. With the presence of Ni^{2+} in the system, Zn^{2+} is able to deposit at a more positive potential, and the nickel potential is shifted cathodically as previously observed in ZnNi systems [57, 62, 79, 82]. As

ZnNi is known to undergo anomalous deposition, the dependence of the metal dissolution peaks relative to one another was expected [48, 50, 65, 68]. The added Mt appeared electrochemically inactive itself and has no overall effect on the anomalous deposition previously observed for ZnNi coating deposition [48].

Though the effect of pH was not discussed in most works, it was studied with the addition of Mt nanoparticles by monitoring the pH of the baths with and without Mt addition over a period of days to determine overall stability of the system. More acidic plating conditions lead to nonuniform coatings, specifically areas of low to no corrosion protection on the underlying substrate [49]. In **Figure 7**, line A represents the system with zinc, nickel and ammonium hydroxide (starting pH = 9.40), line B represents the system with zinc, nickel, ammonium hydroxide and borate (starting pH = 9.40) and line C represents the line with zinc, nickel, ammonium hydroxide, borate and Mt (starting pH = 9.40). The horizontal dot-dash line represents pH 9.21, where the zinc equilibrium species exists (Zn^{2+} and $HZnO_2^-$) [57]. Since this work is based at a pH range near this equilibrium, careful control of the pH is needed throughout all studies. The systems were closed to air for 7 days, then opened to atmosphere and monitored for an additional 32 h. Upon exposure to atmosphere, there was a definite decrease in pH as compared to closed systems for the previously stable baths. Line C (containing Mt in the system) decreased in pH at a slower rate than line B (not containing Mt) suggesting the Mt has an additional effect on the stabilization of metal species in solution. The system without borate or Mt addition passed through pH 9.21 (zinc equilibrium) even as a closed system (Line A). After 7 days the pH of the system with Zn, Ni and NH_4OH had decreased from pH = 9.40 to 9.17, the system with Zn, Ni, borate and NH_4OH had decreased from pH = 9.40 to 9.37 and the system with Zn, Ni, borate, NH_4OH and Mt had decreased

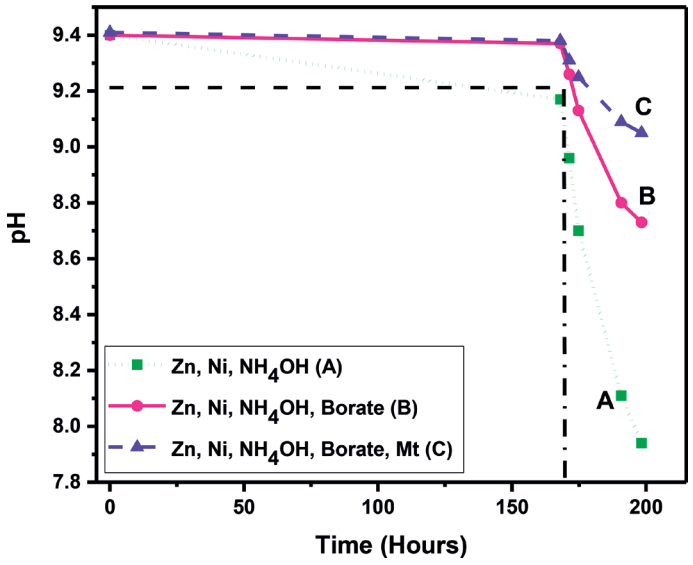


Figure 7. pH studies of electrochemical bath solutions in atmosphere and in a closed system over time. (A) Zn^{2+}, Ni^{2+}, and NH_4OH (dot); (B) Zn^{2+}, Ni^{2+}, 0.1 M borate and NH_4OH (solid); (C) Zn^{2+}, Ni^{2+}, Mt, borate and NH_4OH (dash) [54].

from pH = 9.40 to 9.38. Once opened to atmosphere, it took the borate system 4.5 h to reach a pH of 9.21 and a pH of 8.73 after 32 h, a total decrease of 0.64 pH units. The borate/Mt system reached pH 9.21 after 10 h of exposure to atmosphere and a pH of 9.05 after 32 h, a decrease of 0.33 pH units. The nonstabilized system (no borate or Mt) reached pH 7.94 after 32 h of exposure to atmosphere, a total decrease of 1.46 pH units. The decrease in pH in the closed system is due to formation of metal hydroxide species forming and precipitating out of solution. The large decrease in pH upon exposure to the atmosphere is due to absorption of carbon dioxide from the air [48, 57]. The system with borate demonstrates a clear stabilization of the system when in a closed system, and absorbs CO_2 at a slower rate as compared to the system without borate. The addition of exfoliated Mt nanoparticles further stabilized the system, as shown in the relatively slow pH decrease in this system when closed to air and when opened to atmosphere. The nanoparticles stabilize the pH of the bath improving the deposition of the nanocomposite coating [48].

In the case of ZnNi-Mt nanocomposites, **Figure 8**, XRD pattern had a strong (330) reflection present at 2θ = 42.9°, indicative of ZnNi γ-phase alloy formation with a (330) preferred orientation as previously observed in coatings without nanoparticle incorporation [57, 62, 79]. The coating of pattern B was formed under the same conditions as pattern A, but Mt nanoparticles were dispersed into the electrolyte solution and incorporated into the resulting coating. Since Mt nanoparticles do not give diffraction peaks upon exfoliation, no additional peaks were observed due to its presence [2, 8, 52, 58, 66, 89]. The coating with Mt

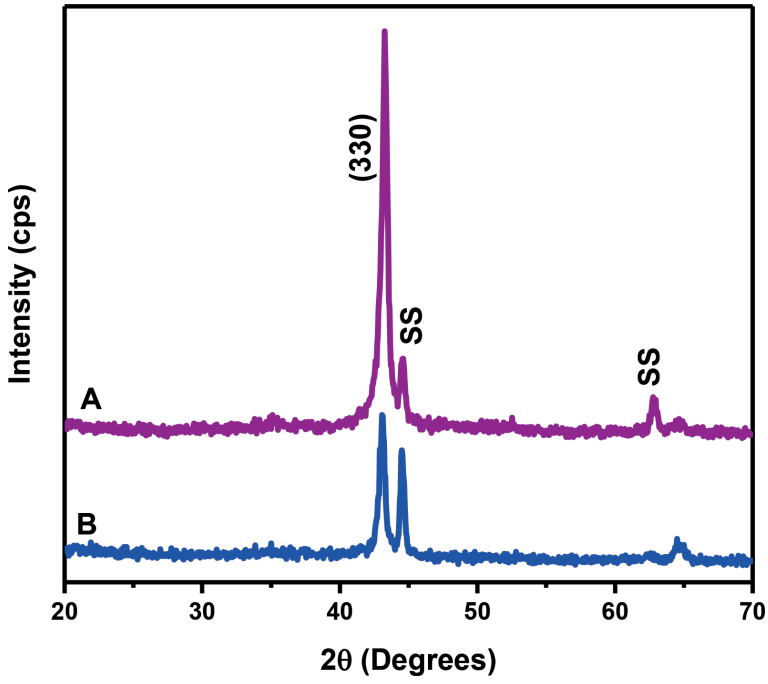


Figure 8. X-ray diffraction patterns of (A) ZnNi and (B) ZnNi Mt scanned from 20 to 70 2Θ at a step size of 0.05° and a dwell time of 1 second [54].

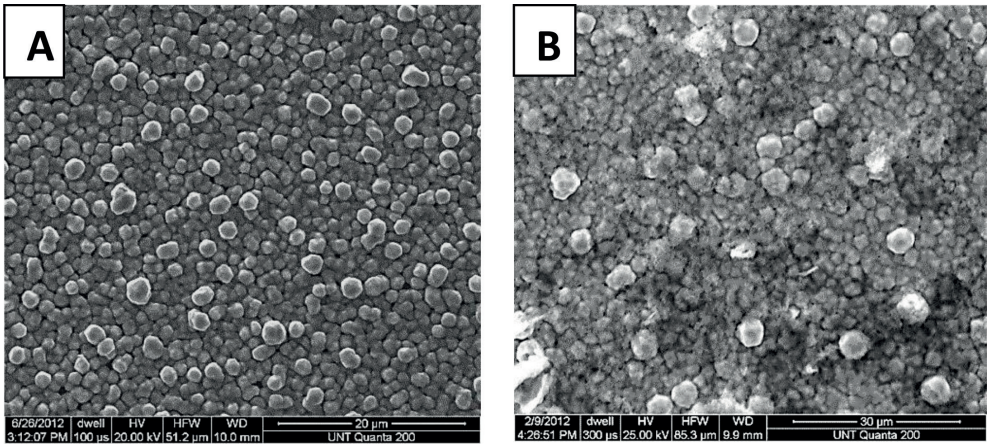


Figure 9. SEM micrographs of (A) ZnNi γ-phase alloy; (B) ZnNi Mt γ-phase nanocomposite alloy [54].

incorporation was thin as compared to the alloy coating without Mt but the γ-phase alloy was still formed even in the presence of Mt, confirming the Mt did not affect the deposition of the alloy phase of interest. The incorporation of Mt into the coating is shown in **Figure 9**. Films with Mt incorporation have strong adherence, small grain size and overall good coverage of the stainless steel substrate. Small spherical particles covered the surface and no voids appeared present in the coating. The structure was not affected by the incorporation of Mt under these conditions. A strong overall coverage of the substrate material was observed, and particles of exfoliated clay were observed, confirming clay presence within the coating.

The potentiodynamic polarization curves of the electrodeposited zinc-nickel and zinc-nickel-Mt nanocomposite alloys in 3.5% NaCl solution are illustrated in **Figure 10** and the corrosion current and potential are given in **Table 4**.

In previous studies ZnNi coatings with optimal corrosion resistance was found to have a corrosion potential (E_{corr}) more anodic as compared to pure zinc but more cathodic as compared to pure nickel. The optimal coatings had a corrosion potential around E = −0.74 V in that study [57]. In this study, the ZnNi-Mt nanocomposite coating had a corrosion potential of E = −0.73 V, which is in agreement with previous findings (**Table 4**). This value is slightly more cathodic (10 mV) than the coatings without Mt incorporation. The high zinc content (~90%) of the coating (confirmed with AAS and ICP-MS) but more cathodic corrosion potential are in the optimal range for improved protection. Corrosion current density is the primary parameter used for evaluating the kinetics of the corrosion reaction. The lower corrosion current density, the better corrosion protection. The corrosion current density for the zinc-nickel γ-phase alloy was 1.06×10^{-5} A/cm^2 and the corrosion current density for the ZnNi-Mt γ-phase nanocomposite alloy was 3.72×10^{-6} A/cm^2. The corrosion current density of the nanocomposite alloy was lower as compared to the alloy without Mt denoting an improved corrosion resistance. R_p of the coating with Mt was 34,900 Ω cm^2 as compared to 30,485 Ω cm^2 for the coating without Mt further confirming the results of improved protection with incorporation of Mt [48].

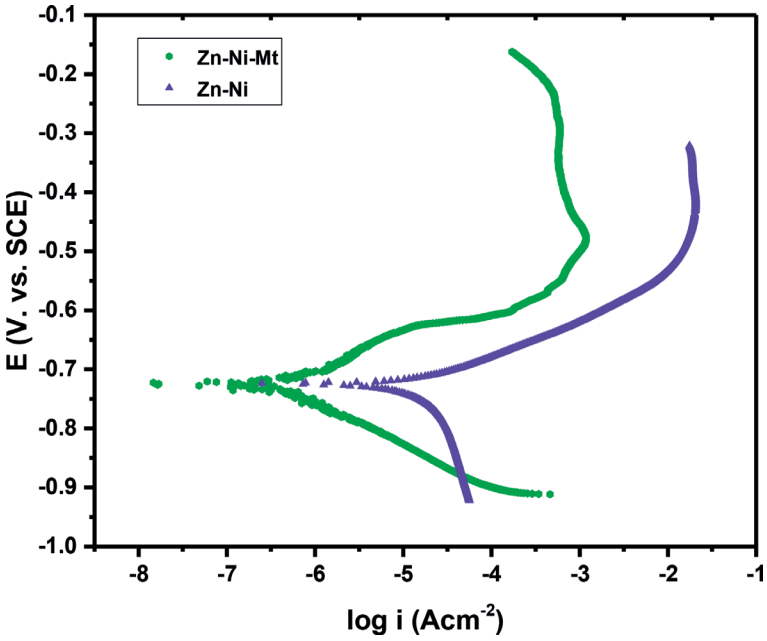


Figure 10. Potentiodynamic polarization curves of ZnNi and ZnNi-Mt nanocomposite coatings, electrolyte NaCl, 3.5 wt %, at scan rate 0.1667 mV/s [54].

5. Conclusions

ZnNi nanocomposites can be formed by incorporating nanoparticles into the coating during an electrochemical deposition. The nanoparticles under study do not appear to affect the electrochemical behavior or electrochemical deposition mechanism of zinc-nickel γ-phase alloy formation. Anomalous deposition of the zinc-nickel alloy was observed which is consistent with formation of the γ-phase alloy, but small anodic shifts were observed in the ALSV scans of the metal species in the ZnNi-Mt bath as compared to baths without Mt nanoparticles present. Al_2O_3 also noted no overall effect on the electrochemical behavior of the system. The addition of nanoparticles, including Mt, SiC and Al_2O_3 also affected the onset of hydrogen evolution, pushing the onset to more cathodic potentials, which can be an advantage in an aqueous plating system as it broadens the working window for the deposition. Zinc-nickel γ-phase deposition requires a high overpotential to overcome the kinetic limitations of nickel deposition, this added benefit of shifting the reduction of the metals anodically with the onset of hydrogen appearing more cathodically, leads to alloy formation with less entrapped hydrogen.

Particle dispersion in the electrolytic bath is an important factor when considering deposition. Optimal corrosion protection is acquired from systems with better dispersion of nanoparticles in the system. When nano-Al_2O_3 particles were dispersed uniformly throughout the coating, and incorporated in the matrix, they were able to protect the coating from corrosive medium, increasing the corrosion potential and retarding corrosion onset. Agglomerated nano-Al_2O_3

particles on the other hand, would combine loosely with the metal matrix, or fall off the coating entirely, leading to gaps and pores in the coating which were easily attacked by corrosion cells. All studies treated the nanoparticles prior to deposition to cause disruption and dispersion of the particles in the plating bath through stirring or sonication, but no studies have been found discussing the overall effect on the particles and any benefits or drawbacks of one method compared to another. It was noted that sonication during deposition leads to better incorporation and higher concentrations of nanoparticles in the final coatings. In addition to sonication, pulse current and pulse potential deposition tends to lead to better incorporation of the nanoparticles in the resulting coating. Up to 11% nanoparticle incorporation was noted throughout the studies, with confirmation of ZnNi-TiO_2, Al_2O_3, SiO_2, SiC, CeO_2, Al_2O_3/SiC, CeO_2/SiO_2, Mt and carbon nanotubes.

XRD results confirm formation of γ-phase ZnNi-nanocomposite coatings throughout the studies. Interestingly, in acidic conditions without nanoparticle incorporation, acidic electrolytic baths tended to give impure ZnNi coatings, with a mixture of γ and δ-phase ZnNi coatings. The studies with ZnNi nanoparticles show almost exclusive γ-phase ZnNi alloys, which previously was primarily observed under alkaline conditions. The crystallite size decreased with the increase of nanoparticle incorporation in the coatings. Mt nanoparticles have been successfully incorporated into the alloy coatings with no disruption in the crystal structure of the zinc-nickel γ-phase alloys, deposited with a preferred (330) orientation. The incorporation of TiO_2, Al_2O_3 and CeO_2 was also confirmed with XRD. The morphology of the coatings shows incorporation of the nanoparticles, with small, compact like structures and few cracks or holes. The hardness of the coatings increased as nanoparticle concentration in the coating was increased.

Corrosion studies all show nanoparticle incorporation into ZnNi coatings leads to lower corrosion currents, suggesting a lower corrosion rate for the coatings. The nanoparticles are believed to fill the crevices, gaps and holes within and on the surface of the coatings, leading to improved corrosion resistance. Overall the corrosion protection offered by the ZnNi-nanocomposite coatings was improved as compared to pure ZnNi coatings.

Author details

Heidi Conrad[1]* and Teresa D. Golden[2]

*Address all correspondence to: h.conrad@tcu.edu

1 Texas Christian University, Fort Worth, Texas, United States

2 University of North Texas, Denton, Texas, United States

References

[1] Musiani M. Electrodeposition of composites: An expanding subject in electrochemical materials science. Electrochimica Acta. 2000;**45**:3397-3402. DOI: 10.1016/S0013-4686(00)00438-2

[2] Tientong J, Ahmad YH, Nar M, D'Souza N, Mohamed AMA, Golden TD. Improved mechanical and corrosion properties of nickel composite coatings by incorporation of layered silicates. Materials Chemistry and Physics. 2014;**145**:44-50. DOI: 10.1016/j.matchemphys.2014.01.025

[3] Szcygiel B, Kolodziej M. Composite Ni/Al_2O_3 coatings and their corrosion resistance. Elecrochim. Acta. 2005;**50**:4188-4195. DOI: 10.1016/j.electacta.2005.01.040

[4] Ciubotariu AC, Benea L, Lakatos-Varsanyi M, Dragan V. Electrochemical impedance spectroscopy and corrosion behaviour of Al_2O_3-Ni nano composite coatings. Electrochimica Acta. 2008;**53**:4557-4563. DOI: 10.1016/j.electacta.2008.01.020

[5] Thurber CR, Ahmad YH, Sanders SF, Al-Shenawa A, D'Souza N, Mohamed AMA, et al. Electrodeposition of 70/30 Cu-Ni nanocomposite coatings for enhanced mechanical and corrosion properties. Current Applied Physics. 2016;**16**:387-396. DOI: 10.1016/j.cap.2015.12.022

[6] Abdulwahab M, Fayomi OSI, Popoola API, Dodo MR. In-situ hybrid study of thermal behaviour of Zn-Ni and Zn-Ni-Al_2O_3 nanocrystallite thin films induced TEA/MEA by electrodeposition. Results in Physics. 2017;**7**:213-215. DOI: 10.1016/j.rinp.2016.11.017

[7] Low CTJ, Wills RGA, Walsh FC. Electrodeposition of composite coatings containing nanoparticles in a metal deposit. Surface and Coating Technology. 2006;**201**:371-383. DOI: 10.1016/j.surfcoat.2005.11.123

[8] Ahmad YH, Tientong J, Nar M, D'Souza N, Mohamed AMA, Golden TD. Characterization and corrosion resistance of electrodeposited Ni-Mo-silicate platelet nanocomposite coatings. Surface and Coating Technology. 2014;**259**:517-525. DOI: 10.1016/j.surfcoat.2014.10.036

[9] Ahmad YH, Tientong J, D'Souza N, Golden TD, Mohamed AMA. Salt water corrosion resistance of electrodeposited Ni-layered silicate nanocomposite coatings from watts' type solution. Surface and Coating Technology. 2014;**242**:170-176. DOI: 10.1016/j.surfcoat.2014.01.040

[10] Roos JR, Celis JP, Fransaer J, Buelens C. The development of composite plating for advanced materials. Journal of Metals. 1990;**11**:60-63. DOI: 10.1007/BF03220440

[11] Momeni MM, Hashemizadeh S, Mirhosseini M, Kazempour A, Hosseinizadeh SA. Preparation, characterization, hardness and antibacterial properties of Zn-Ni-TiO_2 nanocomposite coatings. Surface Engineering. 2016;**32**(7):490-494. DOI: 10.1179/1743294415Y.0000000049

[12] Blejan D, Muresan LM. Corrosion behavior of Zn-Ni-Al_2O_3 nanocomposite coatings obtained by electrodeposition from alkaline electrolytes. Materials and Corrosion. 2013;**64**(5):433-438. DOI: 10.1002/maco.201206522

[13] Tseluikin VN, Koreshkova AA. Synthesis and properties of zinc-nickel-carbon Nanotube composite coatings. Russian Journal of Applied Chemistry. 2016;**89**(6):1027-1030. DOI: 10.1134/s1070427216060288

[14] Hovestad A, Janssen LJJ. Electrochemical codeposition of inert particles in a metal matrix. Journal of Applied Electrochemistry. 1995;**25**:519-527. DOI: 10.1007/BF00573209

[15] Yeh SH, Wan CC. Codeposition of SiC powders with nickel in a watts bath. Journal of Applied Electrochemistry. 1994;**24**:993-1000. DOI: 10.1007/BF00241190

[16] Mohajeri S, Dolati A, Ghorbani M. The photoinduced activity of Ni-TiO_2/TiO_2 multilayer Nanocomposites synthesized by pulse Electrodeposition technique. International Journal of Electrochemical Science. 2017;**12**:5121-5141. DOI: 10.20964/2017.06.50

[17] Li B, Zhang W, Huan Y, Dong J. Synthesis and characterization of Ni-B/Al_2O_3 nanocomposite coating by electrodeposition using trimethylamine borane as boron precursor. Surface and Coating Technology. 2018;**337**:186-197. DOI: 10.1016/j.surfcoat.2018.01.018

[18] Tam J, Jiao Z, Lau JCF, Erb U. Wear stability of superhydrophobic nano Ni-PTFE electrodeposits. Wear. 2017;**374-375**:1-4. DOI: 10.1016/j.wear.2016.12.023

[19] Tang A, Wang M, Huang W, Wang X. Composition design of Ni-nano-Al_2O_3-PTFE coatings and their tribological characteristics. Surface and Coating Technology. 2015;**282**: 121-128. DOI: 10.1016/j.surfcoat.2015.10.034

[20] Frade T, Gomes A, da S, Pereira MI, Alberts D, Pereiro R, et al. Studies on the stability of Zn and Zn-TiO_2 Nanocomposite coatings prepared by pulse reverse current. Journal of the Electrochemical Society. 2011;**158**(3):C63-C70. DOI: 10.1149/1.3531949

[21] Boshkov N, Koleva DA, Petrov P, Tsvetkova N. Corrosion resistant Nano-composite metallic coatings with embedded polymeric aggregates. In: Magagnin L, editor. Engineered Metal Matrix Composites: Forming Methods, Material Properties and Industrial Applications. 1st ed. Hauppauge, N.Y.: Nova Science Publishers; 2013. pp. 261-282. ISBN: 978-1-62081-719-3

[22] Azizi M, Schneider W, Plieth W. Electrolytic co-deposition of silicate and mica particles with zinc. Journal of Solid State Electrochemistry. 2005;**9**:429-437. DOI: 10.1007/s10008-004-0572-3

[23] Praveen BM, Venkatesha TV. Electrodeposition and properties of Zn-nanosized TiO_2 composite coatings. Applied Surface Science. 2008;**254**:2418-2424. DOI: 10.1016/j.apsusc.2007.09.047

[24] Ranganatha S, Venkatesha TV, Vathsala K, Punith kumar MK. Electrochemical studies on Zn/nano-CeO_2 electrodeposited composite coatings. Surface and Coating Technology. 2012;**208**:64-72. DOI: 10.1016/j.surfcoat.2012.08.004

[25] Vathsala K, Venkatesha TV. Zn-ZrO_2 nanocomposite coatings: Electrodeposition and evaluation of corrosion resistance. Applied Surface Science. 2011;**257**:8929-8936. DOI: 10.1016/j.apsusc.2011.05.067

[26] Tuaweri TJ, Wilcox GD. Influence of SiO_2 particles on zinc-nickel electrodeposition. Transactions of the IMF. 2007;**85**(5):245-253. DOI: 10.1179/174591907x229608

[27] Ghaziof S, Gao W. The effect of pulse electroplating on Zn-Ni alloy and Zn-Ni-Al_2O_3 composite coatings. Journal of Alloys and Compounds. 2015;**622**:918-924. DOI: 10.1016/j.jallcom.2014.11.025

[28] Ghaziof S, Gao W. Zn-Ni-Al_2O_3 nano-composite coatings prepared by sol-enhanced electroplating. Applied Surface Science. 2015;**351**:869-879. DOI: 10.1016/j.apsusc.2015.06.010

[29] Ataie SA, Zakeri A. Improving tribological properties of (Zn-Ni)/nano Al_2O_3 composite coatings produced by ultrasonic assisted pulse plating. Journal of Alloys and Compounds. 2016;**674**:315-322. DOI: 10.1016/j.jallcom.2016.02.111

[30] Shourgeshty M, Aliofkhazraei M, Karimzadeh A, Poursalehi R. Corrosion and wear properties of Zn-Ni and Zn-Ni-Al_2O_3 multilayer electrodeposited coatings. Materials Research Express. 2017;**4**:1-13. DOI: 10.1088/2053-1591/aa87d5

[31] Shourgeshty M, Aliofkhazraei M, Karimzadeh A. Study on functionally graded Zn-Ni-Al_2O_3 coatings fabricated by pulse-electrodeposition. Surface Engineering. **2018**:1-10. DOI: 10.1080/02670844.2018.1432172

[32] Zheng HY, An MZ. Electrodeposition of Zn-Ni-Al_2O_3 nanocomposite coatings under ultrasound conditions. Journal of Alloys and Compounds. 2008;**459**:548-552. DOI: 10.1016/j.jallcom.2007.05.043

[33] Zheng HY, An MZ, Lu JF. Surface characterization of the Zn-Ni-Al_2O_3 nanocomposite coating fabricated under ultrasound condition. Applied Surface Science. 2008;**254**:1644-1650. DOI: 10.1016/japsusc.2007.07.110

[34] Gomes A, Almeida I, Frade T, Taveres AC. Zn-TiO_2 and ZnNi-TiO_2 Nanocomposite Coatings: Corrosion Behaviour. Switzerland: Trans Tech Publications; 2010. DOI: 10.4028/www.scientific.net/MSF.636-637.1079

[35] Gomes A, Almeida I, Frade T, Tavares AC. Stability of Zn-Ni-TiO_2 and Zn-TiO_2 nanocomposite coatings in near-neutral sulphate solutions. Journal of Nanoparticle Research. 2012;**14**:692-704. DOI: 10.1007/s11051-011-0692-5

[36] Katamipour A, Farzam M, Danaee I. Effects of sonication on anticorrosive and mechanical properties of electrodeposited Ni-Zn-TiO_2 nanocomposite coatings. Surface and Coating Technology. 2014;**254**:358-363. DOI: 10.1016/jsurfcoat.2014.06.043

[37] Praveen BM, Venkatesha TV. Electrodeposition and corrosion resistance properties of Zn-Ni/TiO_2 Nano composite coatings. International Journal of Electrochemistry. 2001:1-4. DOI: 10.4061/2011/261407

[38] Tuaweri T, Jombo PP, Okpala AN. Corrosion resistance characteristics of Zn-Ni/SiO_2 composite coatings. International Journal of Advanced Science and Engineerin. 2014;**3**(2):1-12. DOI: 10.14810/ijamse.2014.3201

[39] Ullal Y, Hegde C. Corrosion protection of electrodeposited multilayer nanocomposite Zn-Ni-SiO_2 coatings. Surface Engineering and Applied Electrochemistry. 2013;**49**(2):161-167. DOI: 10.3103/S1068375513020142

[40] Takahashi A, Miyoshi Y, Hada T. Effect of SiO_2 colloid on the Electrodeposition of zinc-iron group metal alloy composites. Journal of the Electrochemical Society. 1994;**141**(4): 954-957. DOI: 10.1149/1.2054864

[41] Poliak NI, Anishchik VM, Valko NG, Karwat C, Kozak C, Opielak M. Mechanical properties of Zn-Ni-SiO_2 coating deposited under X-ray irradiation. Acta Physica Polonica, A. 2014;**125**(6):1415-1417

[42] Müller C, Sarret M, Benballa M. ZnNi/SiC composites obtained from an alkaline bath. Surface and Coating Technology. 2002;**162**:49-53. DOI: 10.1016/S0257-8972(02)00360-2

[43] Creus J, Rébéré C, Exbrayat L, Savall C, Fontaine J, Steyer P, et al. Corrosion behavior in saline solution of pulsed electrodeposited Nanocomposite Zn-Ni/CeO_2 coatings. In: Proceedings of the NACE International Conference on International Corrosion Series March 6-10, 2016, Vancouver Canada. December 2017. pp. 1-11

[44] Exbrayat L, Rébéré C, Eyame RN, Steyer P, Creus J. Corrosion behaviour in saline solution of pulsed-electrodeposited zinc-nickel-ceria nanocomposite coatings. Materials and Corrosion. 2017;**68**:1129-1142. DOI: 10.1002/maco.201709419

[45] Tseluikin VN, Koreshkova AA. Electrodeposition of zinc-nickel-carbon Nanotubes composite coatings in a reversing mode. Protection of Metals and Physical Chemistry of Surfaces. 2016;**52**(6):1040-1042. DOI: 10.1134/s2070205116060204

[46] Tulio PC, Rodrigues SEB, Carlos IA. The influence of SiC and Al_2O_3 micrometric particles on the electrodeposition of ZnNi films and the obtainment of ZnNi-SiC and ZnNi-Al_2O_3 electrocomposite coatings from slightly acidic solutions. Surface and Coating Technology. 2007;**202**:91-99. DOI: 10.1016/j.surfcoat.2007.04.084

[47] Xiang T, Zhang M, Li C, Dong C, Yang L, Chan W. CeO_2 modified SiO_2 acted as additive in electrodeposition of Zn-Ni alloy coating with enhanced corrosion resistance. Journal of Alloys and Compounds. 2018;**736**:62-70. DOI: 10.1016/j.jallcom.2017.11.031

[48] Conrad HA. Electrochemically deposited metal alloy-silicate nanocomposite corrosion resistant materials. Ph.D. Dissertation. Denton, TX: University of North Texas; 2013

[49] Rajendran S, Bharathi S, Vasudevan T. The electrodeposition of zinc-nickel alloy from a cyanide-free alkaline plating bath. Transactions of the IMF. 2000;**78**(3):129-133. DOI: 10.1080/00202967.2000.11871324

[50] Fedi B, Gigandet MP, Hihn JY, Mierzejewski S. Structure determination of electrodeposited zinc-nickel alloys: Thermal stability and quantification using XRD and potentiodynamic dissolution. Electrochimica Acta. 2016;**215**:652-666. DOI: 10.1016/j.electacta.2016.08.141

[51] Fratesi R, Roventi G. Electrodeposition of zinc-nickel alloy coatings from a chloride bath containing NH_4Cl. Journal of Applied Electrochemistry. 1992;**22**:657-662. DOI: 10.1007/BF1092615

[52] Lee L, Behera P, Sriraman KR, Chromik RR. The effect of contact stress on the sliding wear behavior of Zn-Ni electrodeposited coatings. Wear. 2018;**400-401**:82-92. DOI: 10.1016/j.wear.2017.12.018

[53] Dingwerth B, Eene van Schaik EG. Cost efficient and high performing: Zinc-alloy corrosion protection for threaded fasteners. Fastener + Fixing Technology, Technical Analysis. Fixing Magazines 2015. Ref. FFT161501/14

[54] El-Sayed AR, Mohran HS, El-Lateef HMA. Corrosion study of zinc, nickel, and zinc-nickel alloys in alkaline solutions by Tafel plot and impedance techniques. Metallurgical and Materials Transactions A: Physical Metallurgy and Materials Science. 2012;**43A**: 619-632. DOI: 10.1007/s11661-011-0908-4

[55] Khan R, Mehmood M, Rizwan R, Ahmad J, Hasan MU, Iqbal Z, et al. Corrosion behavior of zinc-nickel alloy coatings electrodeposited in additive free chloride baths. Corrosion Engineering, Science and Technology. 2001;**46**(7):755-761. DOI: 10.1179/147842210X12741768645794

[56] Gavrila M, Millet JP, Mazille H, Marchandise D, Cuntz JM. Corrosion behaviour of zinc-nickel coatings, electrodeposited on steel. Surface and Coating Technology. 2000;**123** (2-3):164-172. DOI: 10.1016/S0257-8972(99)00455-7

[57] Conrad HA, McGuire MR, Zhou T, Coskun MI, Golden TD. Improved corrosion resistant properties of electrochemically deposited zinc-nickel alloys utilizing a borate electrolytic alkaline solution. Surface and Coating Technology. 2015;**272**:50-57. DOI: 10.1016/j.surfcoat.2015.04.025

[58] Tientong J, Thurber CR, D'Souza N, Mohamed A, Golden TD. Influence of bath composition at acidic pH on electrodeposition of nickel-layered silicate nanocomposites for corrosion protection. International Journal of Electrochemistry. 2013;**853869**:1-8. DOI: 10.1155/2013/853869

[59] Feng Z, Li Q, Zhang J, Yang P, Song H, An M. Electrodeposition of nanocrystalline Zn-Ni coatings with single gamma phase from an alkaline bath. Surface and Coating Technology. 2015;**270**:47-56. DOI: 10.1016/j.surfcoat.2015.03.020

[60] Müller C, Sarret M, Benballa M. Some peculiarities in the codeposition of zinc-nickel alloys. Electrochimica Acta. 2001;**46**:2811-2817. DOI: 10.1016/S0013-4686(01)00493-5

[61] Lehmberg CE, Lewis DB, Marshall GW. Composition and structure of thin electrodeposited zinc-nickel coatings. Surface and Coating Technology. 2005;**192**:269-277. DOI: 10.1016/j.surfcoat.2004.07.109

[62] Conrad HA, Corbett JR, Golden RD. Electrochemical deposition of γ-phase zinc-nickel alloys from alkaline solution. ECS Transactions. 2011;**33**(30):85-95. DOI: 10.1149/1.3566091

[63] Rao VR, Bangera KV, Hegde AC. Magnetically induced electrodeposition of Zn-Ni alloy coatings and their corrosion behaviors. Journal of Magnetism and Magnetic Materials. 2013;**345**:48-54. DOI: 10.1016/j.jmmm.2013.06.014

[64] Tian W, Xie FQ, Wu XQ, Yang ZZ. Study on corrosion resistance of electroplating zinc-nickel alloy coatings. Surface and Interface Analysis. 2009;**41**:251-254. DOI: 10.1002/sia.3017

[65] Ghaziof S, Gao W. Electrodeposition of single gamma phased Zn-Ni alloy coatings from additive-free acidic bath. Applied Surface Science. 2014;**311**:635-642. DOI: 10.1016/j.apsusc.2014.05.127

[66] Horch RA, Golden TD, D'Souza NA, Riester L. Electrodeposition of nickel/montmorillonite layered silicate nanocomposite thin films. Chemistry of Materials. 2002;**14**: 3531-3538. DOI: 10.1021/cm010812+

[67] Kwon M, Jo DH, Cho SH, Kim HT, Park JT, Park JM. Characterization of the influence of Ni content on the corrosion resistance of electrodeposited Zn-Ni alloy coatings. Surface and Coating Technology. 2016;**288**:163-170. DOI: 10.1016/j.surfcoat.2016.01.027

[68] Bajat JB, Maksimović MD, Radović GR. Electrochemical deposition and characterization of zinc-nickel alloys deposited by direct and pulse current. Journal of the Serbian Chemical Society. 2002;**67**(8-9):625-634. DOI: 10.2298/JSC0209625B

[69] Pfiz R, Strub G. A new development for the electrolytic deposition of zinc-nickel alloy with 12-15% nickel from an alkaline bath. Transactions of the IMF. 1996;**74**(5):158-160. DOI: 10.1080/00202967.1996.11871117

[70] Petrauskas A, Grincevičienė L, Česūnienė A, Matulionis E. Stripping of Zn-Ni alloys deposited in acetate-chloride electrolyte under potentiodynamic and galvanostatic conditions. Surface and Coatings Technology. 2005;**192**:299-304. DOI: 10.1016/j.surfcoat.2004.08.191

[71] Wykpis K, Popczyk M, Budniok A. Electrolytic deposition and corrosion resistance of Zn-Ni coatings obtained from sulphate-chloride bath. Bulletin of Materials Science. 2011; **34**(4):997-1001. DOI: 10.1007/s12034-011-0228-8

[72] Magagnin L, Nobili L, Cavallotti PL. Metastable zinc-nickel alloys deposited from an alkaline electrolyte. Journal of Alloys and Compounds. 2014;**615**:S663-S666. DOI: 10.1016/j.jallcom.2014.01.240

[73] Lin YP, Selman R. Electrodeposition of corrosion-resistant Ni-Zn alloy I. Cyclic Voltammetric study. Journal of the Electrochemical Society. 1993;**140**(5):1299-1303. DOI: 10.1149/1.2220974

[74] Bobrikova IG, Kukoz FI, Selivanov VN, Kopin AV. On the zinc-nickel alloy Electrodeposition mechanism. Russian Journal of Electrochemistry. 2002;**38**(10):1148-1151. DOI: 10.1023/A:1020664022224

[75] Roventi G, Cecchini R, Fabrizi A, Bellezze T. Electrodeposition of nickel-zinc alloy coatings with high nickel content. Surface and Coating Technology. 2015;**276**:1-7. DOI: 10.1016/j.surfcoat.2015.06.043

[76] Roventi G, Fratesi R, Della Guardia RA, Barucca G. Normal and anomalous codeposition of Zn-Ni alloys from chloride bath. Journal of Applied Electrochemistry. 2000;**30**: 173-179. DOI: 10.1023/A:1003820423207

[77] Ashassi-Sorkhabi H, Hagrah A, Parvini-Ahmadi N, Manzoori J. Zinc-nickel alloy coatings electrodeposited from a chloride bath using direct and pulse current. Surface and Coating Technology. 2001;**140**:278-283. DOI: 10.1016/S0257-8972(01)01032-5

[78] Oswaldo Pagotto S Jr, Marina de Alverenga Freire C, Ballester M. Zn-Ni alloy deposits obtained by continuous and pulsed electrodeposition processes. Surface and Coating Technology. 1999;**122**:10-13. DOI: 10.1016/S0257-8972(99)00401-6

[79] Conrad H, Corbett J, Golden TD. Electrochemical deposition of γ-phase zinc-nickel alloys from alkaline solution. Journal of the Electrochemical Society. 2012;**159**(1):C29-C32. DOI: 10.1149/2.027201jes

[80] Chandrasekar MS, Pushpavanam M. Pulse and pulse reverse plating- conceptual, advantages and applications. Electrochimica Acta. 2008;**53**:3313-3322. DOI: 10.1016/j.electacta.2007.11.054

[81] Bajat JB, Petrović AB, Maksimović MD. Electrochemical deposition and characterization of zinc-nickel alloys deposited by direct and reverse current. Journal of the Serbian Chemical Society. 2005;**70**(12):1427-1439. DOI: 10.2298/JSC0512427B

[82] Ramanauskas R, Gudavičiūte L, Kaliničenko A, Juškėnas R. Pulse plating effect on micro structure and corrosion properties of Zn-Ni alloy coatings. Journal of Solid State Electrochemistry. 2005;**9**:900-908. DOI: 10.1007/s10008-005-0049-z

[83] Lee L, Behera P, Sriraman KR, Chromik RR. Effects of humidity on the sliding wear properties of Zn-Ni alloy coatings. RSC Advances. 2017;**7**:22662-22671. DOI: 10.1039/c6rs27352a

[84] Monshi A, Foroughi MR, Monshi MR. Modified Scherrer equation to estimate more accurately Nano-crystallite size using XRD. World Journal of Nano Science and Engineering. 2012;**2**:154-160. DOI: 10.4236/wjnse.2012.23020

[85] Langford JI, Wilson JC. Scherrer after sixty years: A survey of some new results in the determination of crystallite size. Journal of Applied Crystallography. 1978;**11**:102-113. DOI: 10.1107/S0021889878012844

[86] Bard AJ, Faulkner LR. Electrochemical Methods: Fundamentals and Applications. 2nd ed. New York: Wiley; 2001; 2000. p. 809. ISBN: 0-471-04372-9

[87] Zhang XL, Jiang ZH, Yao ZP, Song Y, Wu ZD. Effects of scan rate on the potentiodynamic polarization curve obtained to determine the Tafel slopes and corrosion current density. Corrosion Science. 2009;**51**:581-587. DOI: 10.1016/j/corsci.2008.12.005

[88] Armstrong RD, Bell FM. The electrochemical behaviour of zinc in alkaline solution. Electrochemistry. 1974;**4**:1-17

[89] Wang AQ, D'Souza N, Golden TD. Ceramic montmorillonite nanocomposites by electrochemical synthesis. Applied Clay Science. 2008;**42**:310-317. DOI: 10.1016/j.clay.2008.02.004